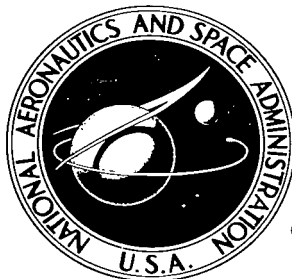


NASA TECHNICAL NOTE



NASA TN D-4005

*e. 1*

LOAN COPY: RETURN  
AFWL (WLIL-2)  
KIRTLAND AFB, N M

0130828



NASA TN D-4005

# STUDY OF CHUGGING INSTABILITY WITH LIQUID-OXYGEN AND GASEOUS-HYDROGEN COMBUSTORS

*by Marcus F. Heidmann, Daniel E. Sokolowski,  
and Lawrence A. Diehl*

*Lewis Research Center  
Cleveland, Ohio*





STUDY OF CHUGGING INSTABILITY WITH LIQUID-OXYGEN  
AND GASEOUS-HYDROGEN COMBUSTORS

By Marcus F. Heidmann, Daniel E. Sokolowski, and Lawrence A. Diehl

Lewis Research Center  
Cleveland, Ohio

NATIONAL AERONAUTICS AND SPACE ADMINISTRATION

---

For sale by the Clearinghouse for Federal Scientific and Technical Information  
Springfield, Virginia 22151 - CFSTI price \$3.00

# STUDY OF CHUGGING INSTABILITY WITH LIQUID-OXYGEN AND GASEOUS-HYDROGEN COMBUSTORS

by Marcus F. Heidmann, Daniel E. Sokolowski, and Lawrence A. Diehl

Lewis Research Center

## SUMMARY

Chugging instability boundaries for a small-scale, liquid-oxygen and gaseous-hydrogen combustion system were experimentally determined over a broad range of operating conditions to establish quantitatively the experimental effect on stability of combustion-system variables. Parallel-jet injection of oxygen into diffusely injected hydrogen was used. Experimental variables included the characteristic combustor length and, for the oxygen system, the number of jets, injector orifice length to diameter ratio, flow-system volume, manifold pressure loss, and atomization mechanism. The experimental results were compared by using the oxygen flow-system pressure drop and the range of stable operation as criteria.

The experimental results were evaluated with the aid of an analytical model that characterizes the combustion process by a time lag (delay time between injection and burning) and an interaction index (sensitivity of combustion processes to pressure oscillations). The analysis showed the stability behavior of the combustor system to be relatively insensitive to the response time of the oxygen flow system. Gas entrainment in liquid oxygen due to local cavitation and/or heat transfer was identified. The average interaction index for all tests was in the range 0 to 0.2. A qualitative model for the breakup time of liquid jets was used to evaluate time-lag variations. Time lag and jet-breakup time appeared to be related to (1) the jet-formation process, which varied with configurations, and (2) the flow properties of the liquid jet and surrounding gas, which varied with operating conditions. An empirical equation based on typical jet-breakup behavior was formulated to give time-lag variations over a range of combustor conditions.

## INTRODUCTION

The results of an experimental study of low-frequency (chugging) instability in a nominal 200-pound-thrust liquid-oxygen and gaseous-hydrogen combustion system are

presented. The study was initiated to investigate flow-system and combustor variables that were known to have or suspected of having an effect on the stability of small-scale experimental combustor systems. Variables in addition to propellant mixture ratio and total flow rate include characteristic combustor length, injector orifice area, injector orifice length to diameter ratio, injector manifold volume, supply line length, and manifold pressure losses. For most of these variables, an effect on stability had been noted, although not fully documented, in previous small-scale experimental programs. In some instances, the effect on stability appeared unexplained or contrary to previously established principles for stability. These variables specifically emphasize the liquid-oxygen flow system. The cryogenic flow system is susceptible to local cavitation and may cause abnormalities in stability characteristics. The cryogenic flow system has been largely ignored in previous experimental studies of chugging instability. A secondary objective of this study was to determine the probable deviations from pure liquid flow.

In the present study, experimental data were acquired to establish quantitatively the effect of the previously mentioned variables on stability. Changes in stability are compared with changes in experimental performance parameters. An analytical model representative of the combustor system is also developed, and the characteristic stability parameters provided by the analysis are used to evaluate the experimental results.

## SYMBOLS

$A$	effective area of flow-system supply line, in. <sup>2</sup>
$\mathcal{A}$	resistance parameter of flow system, $(C_{Di}A_i/C_{Du}A_u)^2$
$A_i$	area of injector orifice, in. <sup>2</sup>
$A_u$	area of upstream orifice, in. <sup>2</sup>
$C_{Di}$	flow coefficient of injector orifice, $\dot{m}_O/A_i(2g\theta \Delta P_i)^{1/2}$
$C_{Du}$	flow coefficient of upstream orifice, $\dot{m}_O/A_u(2g\theta \Delta P_i)^{1/2}$
$c^*$	characteristic exhaust velocity, ft/sec
$\epsilon$	elasticity parameter of flow system, $(2 \Delta P_i \rho l A \epsilon) / \dot{m}_O \theta g$
$f$	frequency, cps
$g$	gravitational constant, ft/sec <sup>2</sup>
$\mathcal{I}$	inertia parameter of flow system, $l \dot{m}_O / (2 \Delta P_i g A \theta g)$
$K_m$	flow resistance, $\Delta P_i / (\dot{m}_O)^2$ , sec <sup>2</sup> /(in. <sup>2</sup> )(lb)
$L^*$	characteristic length of combustor, in.

$L/D$	length to diameter ratio of injector orifice
$L_1, L_2$	function notations
$l$	length of flow-system supply line, in.
$\dot{m}$	mass flow rate, lb/sec
$\dot{m}_H$	mass flow rate of hydrogen, lb/sec
$\dot{m}_O$	mass flow rate of oxygen, lb/sec
$n$	interaction index
$o/f$	oxidant to fuel mass flow rate ratio
$P_c$	combustor pressure, psia
$\Delta P_H$	hydrogen injector orifice pressure drop, psi
$\Delta P_i$	oxygen injector orifice pressure drop, psi
$\Delta P_t$	total oxygen-flow-system pressure drop, psi
$\phi$	pressure-drop parameter of injector orifice, $P_c / (2 \Delta P_i)$
$R$	universal gas constant, 1545 ft-lb/ <sup>o</sup> R(lb mole)
$s$	Laplace transformation parameter
$T_g$	combustion gas temperature, <sup>o</sup> R
$t$	time, sec
$U_H$	velocity of unburnt hydrogen in combustor, ft/sec
$U_O$	oxygen jet velocity, ft/sec
$Y$	position of concentrated flow-system elasticity
$z$	dimensionless time, $t/\theta_g$
$\delta$	dimensionless time lag, $\tau/\theta_g$
$\epsilon$	compressibility of flow-system fluid, $\text{psi}^{-1}$
$\eta_c$	characteristic velocity efficiency
$\theta_g$	mean gas residence time in combustor, sec
$\lambda$	real part of Laplacian operator when $s = \lambda + i\omega$
$\mu_i$	fractional flow perturbation, $\left[ (\dot{m}_O - \bar{\dot{m}}_O) / \bar{\dot{m}}_O \right] (z)$
$\mu_i'$	fractional flow perturbation with retarded action, $\left[ (\dot{m}_O - \bar{\dot{m}}_O) / \bar{\dot{m}}_O \right] (z - \delta)$
$\rho$	density of oxygen, lb/ft <sup>3</sup>

- $\rho_g$  density of combustion gases, lb/ft<sup>3</sup>
- $\tau$  total time lag from instant of injection to instant of combustion of a propellant element, sec
- $\tau_j$  liquid-jet-breakup time, sec
- $\varphi$  fractional pressure perturbation,  $\left[ (P_c - \bar{P}_c) / \bar{P}_c \right] (z)$
- $\varphi'$  fractional pressure perturbation with retarded action,  $\left[ (P_c - \bar{P}_c) / \bar{P}_c \right] (z - \delta)$
- $\omega$  dimensionless frequency

Superscript:

( $\bar{\quad}$ ) mean steady-state value

## COMBUSTION AND FLOW SYSTEMS

### Test Facility

Various combustor configurations were evaluated in an experimental rocket test facility equipped with gaseous-hydrogen and liquid-oxygen flow systems. A schematic diagram of these flow systems is presented in figure 1. Both the fuel and oxidizer systems utilized a pressure-regulated feed to control flow rates. The mass flow rate of hydrogen to the combustor was metered by a critical-flow venturi. Liquid oxygen was supplied from a pressurized tank immersed in a liquid-nitrogen bath. A cooling coil, turbine-type flowmeter, and propellant valve were also immersed in liquid nitrogen to assure a constant low-temperature supply of oxygen. Nominal flow rates ranged as high as 1.0 pound per second for oxygen and 0.25 pound per second for hydrogen. Lengths and volumes of feed lines are also shown in figure 1. The length of the liquid-oxygen supply line past station 3, hereinafter referred to as the liquid-oxygen manifold, is discussed in greater detail in a later section.

### Combustor Configuration

The experimental rocket combustor, shown in figure 2, was nominally rated at 200 pounds thrust and a chamber pressure of 400 pounds per square inch absolute. An uncooled copper combustion chamber, with an internal diameter of 2 inches, was fabricated in sections to facilitate interchanging several chamber lengths. The nozzle was constructed with a 3-inch convergent section and a water-cooled throat. A mean nozzle-throat diameter of 0.62 inch gave a contraction ratio of 10.4. As shown in figure 3,

gaseous hydrogen was injected in a diffuse manner through a multihole plate that spread the hydrogen throughout the chamber cross section. This hydrogen system was held constant, and design parameters for the liquid-oxygen system were changed. The liquid-oxygen manifold and injector are shown in figure 4. A variable number of closely spaced rows of 0.040-inch-diameter jets consisting of 20 jets per row produced a showerhead stream parallel to the longitudinal axis of the chamber. The resultant pattern was essentially a sheet of liquid oxygen surrounded by gaseous hydrogen. With this design, the manifold and orifice configuration could be changed without substantially affecting the basic injection pattern or chamber geometry.

## Reference Configuration

The configuration changes selected for study were deviations from a basic or reference configuration. The chamber length for this reference configuration was chosen to give an  $L^*$  of 156 inches, while the liquid-oxygen injector and manifold are as depicted in figures 5 and 6(a). The basic injector consisted of two rows of 20 equally spaced orifices. All design parameters that were studied were variations of the reference configuration.

## Combustor Configuration Variables

Characteristic length of combustor. - Characteristic length  $L^*$  was varied to study changes in the mean gas residence time  $\theta_g$ . The residence time is related to  $L^*$  by the relation  $\theta_g = L^*c^*/gRT_g$ . This residence time is a characteristic parameter of an unstable combustor (ref. 1). Characteristic combustor lengths of 81 and 224 inches were used to study the effect of both increasing and decreasing  $\theta_g$ .

Length to diameter ratio of injector orifice. - Jet-length variations (figs. 6(b) and (c)) were examined for changes in orifice flow characteristics. Two longer  $L/D$  ratios of 3.90 and 6.25 were compared with the reference  $L/D$  of 1.56.

Number of jets. - The number of oxygen orifices (jets) was increased to 60 and decreased to 20 to vary the distribution of pressure drop and jet velocity at a constant total flow rate. These changes are depicted in figures 6(d) and (e).

Flow-system volume. - The volume of the liquid-oxygen cavity (fig. 6(f)) was increased from 0.25 to 1.56 cubic inches by increasing the cavity diameter from 1/4 to 5/8 inch. The larger cavity increased the flow-system capacitance at the injector and also gave lower values of jet-entrance cross velocity; both these could give significant effects on chugging stability.

The volume of the supply manifold was increased from 2.85 to 3.90 cubic inches by extending the manifold side branch from 5 to 12 inches. This increased volume gave a significant change in overall flow-system capacitance that could affect stability.

Diameter of upstream orifice. - Upstream orifice diameter was reduced from 0.070 to 0.052 inch to test the effect of a change in pressure-drop distribution within the overall flow system. This reduction of orifice diameter simulates a change in manifold pressure losses. Such losses are frequently encountered in injector designs and contribute to system stability.

Splash plate. - A splash plate was affixed to the reference injector (fig. 6(g)) to produce a large change in the atomization and dispersion of the oxygen. The splash plate was used to test the effect on system stability of a significant change in the combustion process.

## EXPERIMENTAL EVALUATIONS

### Combustor Test Procedure

Combustor performance was evaluated during runs in which propellant mass flow rates, supply pressures, and static as well as dynamic pressures were the primary performance measurements. The procedure for obtaining data was as follows: Hydrogen flow rate was held constant and oxygen flow rate was varied until the region between stable and unstable operation was well defined. This procedure was repeated at four different hydrogen flow rates until a stability boundary was established for each configuration.

Overall flow-system pressure drops were measured for each operating condition. Injector pressure drops used in this study were established in nonburning tests, and the deviation from burning conditions is unknown. Injector pressure-drop measurements attempted during test firings were unreliable because (1) the low pressure drops of the injector could not be established accurately at the operating pressure of the system and (2) the insertion of a transducer in the manifold caused changes in the stability of the system.

Liquid-oxygen temperature was measured during burning tests by inserting a thermocouple in the injector manifold. The average temperature was  $-305^{\circ}$  F, which corresponds to a density of 0.0421 pound per cubic inch.

### Experimental Results

Experimental data for the reference combustor configuration are shown in figures 7

to 9. Combustion pressure is displayed in figure 7 as a function of the ratio of mass flow rates  $o/f$  for the four hydrogen flow rates. Pressure drops across the hydrogen injection system exclusive of the critical-flow nozzle are also shown. A stability boundary was established by a line separating the stable and unstable conditions into two regions. Figure 8 is a cross plot of these results where combustion pressure and the stability boundary are presented as functions of oxygen and hydrogen flow rates. Also shown on this performance map are the oxygen injector-orifice pressure drop  $\Delta P_i$ , total oxygen flow-system pressure drop  $\Delta P_t$ , and the oscillatory frequency of the system at conditions along the stability boundary. Figure 9 shows the experimental data used to establish these oscillatory frequencies. Figure 10 is a performance map that displays computed values of  $c^*$  efficiency,  $\eta_c$ , over the range of test conditions.

Experimental data for all combustor configurations were evaluated in a similar manner. The performance maps for these configurations are shown in figures 11 and 12.

## COMPARISON OF EXPERIMENTAL RESULTS

### Monopropellant Behavior

In comparing the experimental results of the various configurations, it will be assumed that perturbations in hydrogen flow rate due to combustor pressure oscillations have a negligible effect on stability compared with the effect of perturbations in oxygen flow rate. Relative insensitivity to hydrogen flow perturbations can be justified for the injector configurations and mixture ratios used in these tests. Gaseous hydrogen was diffusely injected upstream of the oxygen orifices at a relatively high pressure drop and at a rate exceeding stoichiometric proportions. With such gaseous injection, any perturbation in flow rate at the point of injection diffuses rapidly and does not at some later time cause a corresponding flow perturbation at the position of burning; however, a small perturbation in the total mass of hydrogen in the combustor can occur. Such a perturbation has a reduced and negligible effect on combustor pressure because hydrogen in excess of that needed for chemical conversion prevails at all times. The dynamic behavior of the combustor system, therefore, is predominantly that of a monopropellant (oxygen) system with the bipropellant effects confined to establishing mean values of pressure, flow rate, and other parameters.

### Method of Comparison

Although various comparisons of the performance maps of figures 11 and 12 can be

made, the experimental effect of configuration changes on stability will be examined by using properties that characterize the oxygen flow system and the combustion system. The properties and the reason for comparing these properties are given in the following paragraphs.

Oxygen flow rates. - One measure of the stability of a combustor is the range of operating conditions that provides stable operation. The oxygen flow rate at the stability boundary is an index of the extent of the stable operating region; that is, a configuration change causing a decrease in this oxygen flow rate indicates an increased range of stable operation. For simplicity, the comparisons are restricted to the oxygen flow rate at a combustor pressure of 350 pounds per square inch absolute along the stability boundary; this is a condition that adequately represents each configuration.

Mixture ratio. - Mixture ratio is a generally used performance parameter and is related to oxygen flow rate at a pressure of 350 pounds per square inch absolute along the stability boundary. This parameter will also be used to indicate the extent of the stable operating region. As in the case of flow rate, a decrease in mixture ratio indicates an improvement in stability.

Total pressure-drop parameter. - For steady flow, the oxygen flow process can be characterized by the relation

$$\frac{\Delta P_t}{(\dot{m}_O)^2} = K_m$$

which for small perturbations gives the relation

$$\frac{\dot{m}_O - \bar{\dot{m}}_O}{\bar{\dot{m}}_O} = \frac{P_c}{2 \Delta P_t} \left( \frac{P_c - \bar{P}_c}{\bar{P}_c} \right)$$

The parameter  $P_c/(2 \Delta P_t)$  is an index of the magnitude of a flow perturbation caused by a pressure perturbation and, when sufficiently small, will generally ensure stability in a combustor system. The values of  $P_c/(2 \Delta P_t)$  required for stability will differ for various combustor systems because of interacting effects that are inherent in the overall system. A comparison of  $P_c/(2 \Delta P_t)$  at the stability boundary of two combustors, therefore, indicates the difference in their inherent stability; the combustor with a large value of  $P_c/(2 \Delta P_t)$  is inherently more stable. The configurations are compared by using this index, with the comparison again being restricted to a combustor pressure of 350 pounds per square inch absolute.

Resistance parameter. - The resistance parameter  $K_m$  is a measure of the total

resistance to steady flow of the oxygen flow system. Changes in this parameter indicate changes in the flow system. Although  $K_m$  is a function of the flow area, its value is affected also by pressure recovery factors, coefficients of discharge, and viscous and other flow losses. Values of  $K_m$  for different configurations will be compared to indicate changes in resistance; a large value of  $K_m$  indicates a large resistance.

Coefficient of discharge. - Values of the coefficient of discharge of the injector orifices  $C_{Di}$  will also be compared. Although  $C_{Di}$  is incorporated in  $K_m$ , a change in  $C_{Di}$  indicates a change in the discharge of oxygen from the injector that could affect propellant preparation and the combustion rate.

Combustor efficiencies. - Combustor efficiency is an index of the burning process. In this study, two variables that have important effects on burning rate are (1) a change in configuration and (2) a change in propellant flow rate. The efficiency  $\bar{\eta}_c$  evaluated at mean oxygen and hydrogen flow rates of 0.3 and 0.15 pound per second, respectively, are compared to indicate the effect of a configuration change on the burning process independent of changes in stability. The efficiency  $\eta_c$  evaluated at a combustor pressure of 350 pounds per square inch absolute at the stability boundary will also be considered, because flow rates at this condition vary substantially with changes in stability. This efficiency is a measure of the burning process for the flow-rate conditions that prevail at the stability boundary.

## Effect of Combustor Configuration Variables on Stability

In the following tables, the previously discussed parameters for each configuration variable are compared with those for the reference combustor configuration. An increase or decrease in stability relative to the reference configuration is tabulated. The range of the stable operating region and the inherent stability, indicated by  $\dot{m}_O$  and  $P_c/2 \Delta P_t$ , respectively, are used in the stability rating. The tables are generally self-explanatory; however, several remarks about flow and combustion-system behavior are included.

Characteristic length of combustor:

Configuration variable, $L^*$	System parameter							Stability	
	$\dot{m}_O$	o/f	$P_c/(2 \Delta P_t)$	$K_m$	$C_{Di}$	$\eta_c$	$\bar{\eta}_c$	Range	Inherent
81	0.417	3.35	1.79	563	0.505	77	78	Decrease	Decrease
156 (reference)	.37	3.47	2.24	563	.505	85	88	-----	-----
224	.36	3.18	2.34	563	.505	87	90	Increase	Increase

The combustion process changed with  $L^*$  because of the change in the length and volume for combustion.

Length to diameter ratio of injector orifice:

Configuration variable, L/D	System parameter							Stability	
	$\dot{m}_O$	o/f	$P_c/(2 \Delta P_t)$	$K_m$	$C_{Di}$	$\eta_c$	$\bar{\eta}_c$	Range	Inherent
1.56 (reference)	0.37	3.47	2.24	563	0.505	85	88	-----	-----
3.90	.33	2.65	2.57	570	.620	92	93	Increase	Increase
6.25	.335	2.65	2.82	552	.675	88	89	Increase	Increase

The combustion-process and injector-discharge changes with L/D may be related effects.

Number of jets:

Configuration variable, number of jets	System parameter							Stability	
	$\dot{m}_O$	o/f	$P_c/(2 \Delta P_t)$	$K_m$	$C_{Di}$	$\eta_c$	$\bar{\eta}_c$	Range	Inherent
20	0.33	2.36	2.24	715	0.509	87	87	Increase	No change
40 (reference)	.37	3.47	2.24	563	.505	85	88	-----	-----
60	.415	4.80	1.67	610	.568	84	80	Decrease	Decrease

The flow-system resistance increased with 20 jets because of the reduced flow area. Injector-discharge, combustion-process, and flow-system-resistance changes with 60 jets indicate a significant change in flow-system behavior and propellant preparation.

Flow-system volume:

Configuration variable, flow system volume	System parameter							Stability	
	$\dot{m}_O$	o/f	$P_c/(2 \Delta P_t)$	$K_m$	$C_{Di}$	$\eta_c$	$\bar{\eta}_c$	Range	Inherent
Reference	0.37	3.47	2.24	563	0.505	85	88	-----	-----
Large injector cavity	.315	2.3	2.36	745	.680	90	91	Increase	Increase
Extended manifold	.38	3.6	1.77	685	.505	83	82	Decrease	Decrease

The increase in flow-system resistance with an increase in volume may indicate a change in gas entrainment due to heat transfer and/or cavitation. The change in the combustion process may be related but shows no consistent trend with the volume change.

Diameter of upstream orifice:

Configuration variable, diameter of upstream orifice	System parameter							Stability	
	$\dot{m}_O$	o/f	$P_c/(2 \Delta P_t)$	$K_m$	$C_{Di}$	$\eta_c$	$\bar{\eta}_c$	Range	Inherent
0.052	0.24	0.94	1.23	2460	0.505	94	86	Increase	Decrease
.070 (reference)	.37	3.47	2.24	563	.505	85	88	-----	-----

The flow-system resistance increased because of the small orifice.

Splash plate:

Configuration variable, splash plate	System parameter							Stability	
	$\dot{m}_O$	o/f	$P_c/(2 \Delta P_t)$	$K_m$	$C_{Di}$	$\eta_c$	$\bar{\eta}_c$	Range	Inherent
Without splash plate (reference)	0.37	3.47	2.24	563	0.505	85	88	-----	-----
With splash plate	.22	.96	3.58	102	.505	98	94	Increase	Increase

The change in propellant preparation was effective in changing the combustion process. Flow-system resistance was affected by the splash plate.

### Composite Comparison of Combustor Configuration Variables

In the following table, the configuration variables are listed in the order of their rel-

Configuration variable	Inherent stability, $P_c/(2 \Delta P_t)$	Oxidant to fuel mass flow rate ratio, o/f	Rank according to stability rating
With splash plate	3.58	0.96	2
Length to diameter ratio, 6.25	2.82	2.59	5
Length to diameter ratio, 3.9	2.57	2.73	6
Large injector cavity	2.36	2.30	3
Characteristic length, 224 in.	2.34	3.14	7
20 Jets	2.24	2.36	4
Reference	2.24	3.47	9
Characteristic length, 81 in.	1.79	3.35	8
Extended manifold	1.77	3.60	10
60 Jets	1.67	4.80	11
Upstream orifice diameter, 0.052 in.	1.23	0.92	1

ative inherent stability. The range of the stable operating region (as indicated by the  $\sigma/f$ ) is shown, and the rank according to this stability rating is noted. The 0.052-inch upstream-orifice configuration is the only configuration that is rated significantly different by the two rating methods. This comparison of the configurations shows the design features that provide the greatest stability. However, the validity of combining all these design features in a single configuration to obtain stability must be questioned because interacting effects can occur. Since these experimental effects have limited application to other combustors, additional qualitative and quantitative evaluations were made by employing an analytical model to interpret these data.

## THEORETICAL ANALYSIS OF RESULTS

The existing analytical models for low-frequency combustion instability (refs. 1 to 6) are interrelations of response functions for both the flow and combustion systems. In these models, a combustion time lag is generally postulated to characterize a property of the combustion process. In reference 1, a more realistic representation is attained by also postulating an interaction index. This index accounts for variations in combustion rates caused by physical and chemical kinetic changes due to chamber and injector geometry, types of propellants, etc., between one combustor design and another. In the present analysis, the analytical derivations presented in reference 1 are used. The analytical description of the flow system is expanded, however, to include the effect of a discrete feedline pressure drop, as represented by the upstream orifice in the experimental configurations.

### Analytical Model

A schematic diagram of the oxygen flow system considered for analytical study is shown in figure 13. The propellant flow originates from a constant-pressure supply tank and incurs orifice-type pressure drops at both the tank outlet and the entrance to the combustion chamber. Liquid capacitance and inertia are considered to be important only in the flow line between the two orifices. However, the capacitance is assumed to exist at a point source.

The dimensionless equation that describes the flow-system dynamics is given as follows:

$$\mathcal{P} \left( 1 + \mathcal{E} \mathcal{A} \frac{d}{dz} + \mathcal{I} \mathcal{E} Y \frac{d^2}{dz^2} \right) \varphi + \left\{ 1 + \mathcal{A} + (\mathcal{E} \mathcal{A} + \mathcal{I}) \frac{d}{dz} + [\mathcal{I} \mathcal{E} (1 - Y) \mathcal{A} + \mathcal{I} \mathcal{E} Y] \frac{d^2}{dz^2} + \mathcal{I}^2 \mathcal{E} Y (1 - Y) \frac{d^3}{dz^3} \right\} \mu_i = 0 \quad (1)$$

where  $\mathcal{E}$ ,  $\mathcal{I}$ , and  $\mathcal{P}$  are the elasticity, inertia, and pressure-drop parameters, respectively, of the flow system and are defined by the following relations:

$$\mathcal{E} = \frac{2 \Delta \bar{P}_i \rho l A \epsilon}{\dot{m} \theta_g}; \quad \mathcal{I} = \frac{\bar{l} \dot{m}}{2 \Delta \bar{P}_i g A \theta_g}; \quad \mathcal{P} = \frac{\bar{P}_c}{2 \Delta \bar{P}_i}$$

The resistance parameter  $\mathcal{A}$ , which is defined as

$$\mathcal{A} = \left( \frac{C_{Di} A_i}{C_{Du} A_u} \right)^2 \quad (2)$$

is the modifying factor between equation (1) and the equation presented in reference 1. Equation (1) relates the fractional perturbation in propellant injection  $\mu_i$  to the fractional perturbations in chamber pressure  $\varphi$ .

The dimensionless equation that describes the combustion system dynamics as derived in reference 6 is

$$\frac{d\varphi}{dz} + \varphi = \mu_i' + n(\varphi - \varphi') \quad (3)$$

where  $n$  is the pressure index of interaction and the primed parameters are functions of a retarded time,  $z - \delta$ . By following the procedure of reference 1, the magnitude of the perturbations  $\mu_i$  and  $\varphi$  in equation (1) are assumed to be the same as the primed term perturbations in equation (3), and the two equations are combined by elimination of  $\mu_i'$ . Thus,

$$\left(1 - n + \frac{d}{dz}\right)\varphi = - \left\{ \frac{\mathcal{P}(1 + \mathcal{E}\mathcal{A}) \frac{d}{dz} + \mathcal{J}\mathcal{E}Y \frac{d^2}{dz^2}}{1 + \mathcal{A} + (\mathcal{E}\mathcal{A} + \mathcal{J}) \frac{d}{dz}} + [\mathcal{J}\mathcal{E}(1 - Y)\mathcal{A} + \mathcal{J}\mathcal{E}Y] \frac{d^2}{dz^2} + \mathcal{J}^2\mathcal{E}Y(1 - Y) \frac{d^3}{dz^3} \right\} \varphi' - \frac{1}{n} \varphi' \quad (4)$$

This equation is of the form

$$L_1\left(\frac{d}{dz}\right)\varphi = L_2\left(\frac{d}{dz}\right)\varphi' \quad (5)$$

and from reference 6 has a solution in Laplace notation of the form

$$L_1(s) = e^{-s\delta} L_2(s) \quad (6)$$

Solving equation (4) by comparison with equation (6) yields the following general equation which gives the dynamic relation between the flow system and the combustion system:

$$(1 - n + s + ne^{-s\delta}) \left\{ 1 + \mathcal{A} + (\mathcal{E}\mathcal{A} + \mathcal{J})s + [\mathcal{J}\mathcal{E}(1 - Y)\mathcal{A} + \mathcal{J}\mathcal{E}Y]s^2 + \mathcal{J}^2\mathcal{E}Y(1 - Y)s^3 \right\} + \mathcal{P}(1 + \mathcal{E}\mathcal{A}s + \mathcal{J}\mathcal{E}Ys^2)e^{-s\delta} = 0 \quad (7)$$

The condition of neutral stability is defined when the real part  $\lambda$  of the complex conjugate root  $s = \lambda + i\omega$  is equal to zero. Solutions for neutral stability are obtained when the real and imaginary parts of equation (7) are equated to zero. Two specific solutions are of interest in this study; one is for the capacitance concentrated at the injector ( $Y = 1$ ), and the other is for the capacitance at the upstream orifice ( $Y = 0$ ). For  $Y = 1$ ,

$$\left[(1 - n)^2 + \omega^2\right] \left[ (\mathcal{A} + 1 - \mathcal{J}\mathcal{E}\omega^2)^2 + (\mathcal{A}\mathcal{E}\omega + \mathcal{J}\omega)^2 \right] = \left[ n\mathcal{A} + (n + \mathcal{P})(1 - \mathcal{J}\mathcal{E}\omega^2) \right]^2 + \left[ n\mathcal{J}\omega + (n + \mathcal{P})\mathcal{A}\mathcal{E}\omega \right]^2 \quad (8)$$

$$\delta = \frac{1}{\omega} \left\{ \pi - \tan^{-1}\left(\frac{\omega}{1 - n}\right) - \tan^{-1}\left(\frac{\mathcal{A}\mathcal{E}\omega + \mathcal{J}\omega}{\mathcal{A} + 1 - \mathcal{J}\mathcal{E}\omega^2}\right) + \tan^{-1}\left[\frac{(n + \mathcal{P})\mathcal{A}\mathcal{E}\omega + n\mathcal{J}\omega}{n\mathcal{A} + (n + \mathcal{P})(1 - \mathcal{J}\mathcal{E}\omega^2)}\right] \right\} \quad (9)$$

and for  $Y = 0$ ,

$$\left[ (1-n)^2 + \omega^2 \right] \left[ (1 + \mathcal{A} - \mathcal{J}\mathcal{A}\mathcal{E}\omega^2)^2 + (\mathcal{A}\mathcal{E}\omega + \mathcal{J}\omega)^2 \right] = \left[ n(1 + \mathcal{A} - \mathcal{J}\mathcal{A}\mathcal{E}\omega^2) + \mathcal{P} \right]^2 + \left[ (n + \mathcal{P})\mathcal{A}\mathcal{E}\omega + n\mathcal{J}\omega \right]^2 \quad (10)$$

$$\delta = \frac{1}{\omega} \left\{ \pi - \tan^{-1} \left( \frac{\omega}{1-n} \right) - \tan^{-1} \left( \frac{\mathcal{A}\mathcal{E}\omega + \mathcal{J}\omega}{\mathcal{A} + 1 - \mathcal{J}\mathcal{A}\mathcal{E}\omega^2} \right) + \tan^{-1} \left[ \frac{(n + \mathcal{P})\mathcal{A}\mathcal{E}\omega + n\mathcal{J}\omega}{n(\mathcal{A} + 1 - \mathcal{J}\mathcal{A}\mathcal{E}\omega^2) + \mathcal{P}} \right] \right\} \quad (11)$$

For each of the two cases, solutions for  $\delta$  are obtained by simultaneously satisfying both corresponding equations.

## Analytical Solutions

Solutions for  $\delta$  along the stability boundaries shown in figure 11 are only possible for known values of either  $n$  or  $\mathcal{E}$ . The interaction index  $n$  characterizes the combustion dynamics and is not specified by the experimental measurements. The elasticity  $\mathcal{E}$  is considered unknown because of the probability of gas entrainment in the cryogenic flow system. Discrete points along the stability boundaries, therefore, have a range of probable solutions for  $\delta$ . Solutions for  $\delta$  and  $\mathcal{E}$  for assumed values of  $n$  were obtained by iteration on a high-speed digital computer. The related dimensional quantities of time lag  $\tau$  and liquid compressibility  $\epsilon$  for these solutions are given in table I.

For a typical operating condition figure 14 shows the relation between  $n$ ,  $\tau$ , and  $\epsilon$  given by these solutions. Solutions for  $Y = 0$  and  $Y = 1$  are shown. For both these solutions, an upper-limit value of  $n$  is obtained when liquid compressibility is equal to zero. Realistically,  $n$  must be less than the value corresponding to liquid compressibility for oxygen with no gas entrainment ( $10 \times 10^{-6} \text{ psi}^{-1}$ ), as noted in figure 14. Other operating conditions shown in table I exhibit a similar relation between  $n$  and  $\tau$ ; however, the limiting value of  $n$  for some conditions is less than zero. Negative values of  $n$  give valid solutions for these conditions, but the numerical evaluations were not made in this study.

## DISCUSSION OF ANALYTICAL SOLUTIONS

### Position of Flow-System Elasticity

Table I presents solutions for the reference combustor configuration with the flow-

system elasticity assumed concentrated at the injector  $Y = 1$  and at the upstream orifice  $Y = 0$ . Figure 14 shows these solutions for one operating condition. Differences in the solutions for  $Y = 1$  and  $Y = 0$  are negligible for this and all other configurations. It is concluded that stability is insensitive to the position of any local cavitation or gas entrainment in the flow system. The effective position of such a gas inclusion, therefore, cannot be identified from the stability data.

This insensitivity to position is attributed to the dynamics of the particular flow system used for the experimental tests. An evaluation of the phase-angle terms in equations (9) and (11) shows that the delay between a combustor pressure change and a flow change is small compared with the period of oscillation. This causes the stability of the overall combustor system to be relatively insensitive not only to the position but also to small changes in flow-system capacitance.

### Composite Evaluation of Interaction Index and Time Lag

Since both the flow-system elasticity and the interaction index are unknown, unique values of  $\tau$ ,  $\epsilon$ , and  $n$  for each test condition cannot be established. Some insight into the behavior of the combustion and flow systems can be acquired, however, by analyzing the solutions for two conditions; these are (1) a constant liquid compressibility and (2) a constant interacting index.

Interaction index. - Values of interaction index are obtained for each operating condition when liquid compressibility is taken as that of liquid oxygen without gas entrainment ( $10 \times 10^{-6} \text{ psi}^{-1}$ ). These values of interaction index range between approximately 0.7 and 0 and are shown as a function of combustor pressure in figure 15. Solutions for the splash-plate configuration were not evaluated but are known to be negative. The curves in figure 15 represent individual configurations. Although some increase in the index with pressure is noted for each configuration, the interaction index does not appear to be a unique function of pressure. The dispersion of values shown in figure 15 implies that the pressure sensitivity of the combustion process as indicated by the parameter  $n$  must vary with operating conditions and configuration changes in order that the assumption of a constant compressibility be valid.

A similar dispersion of results is obtained for a constant compressibility other than that for liquid oxygen. Assuming a liquid compressibility greater than that of liquid oxygen gives smaller values of interaction index, as shown in table I and demonstrated in figure 14. The values of interaction index shown in figure 15, therefore, are the highest possible values for each condition (since compressibility less than that for liquid oxygen is impossible). Hence, any comparison of results made on the basis of a constant interaction index must be made for an index at or near zero if the comparison is to encompass all test conditions.

Probable variations in liquid compressibility may be examined in a similar manner. Values of liquid compressibility are obtained for each operating condition when interaction index is assumed constant. Figure 16 shows these values of liquid compressibility for  $n = 0$  as a function of injector manifold pressure with the curves again relating data for each configuration. Although a large dispersion of results is obtained, a decrease in compressibility with an increase in pressure is apparent when characteristics of individual configurations are analyzed. This trend is consistent with the properties of a two-phase medium, as shown by the lines of constant volume percent gas in the flow system in figure 16. Gas entrainment of less than 2 percent of the flow-system volume could account for the values of compressibility needed to satisfy analytical solutions for an interaction index of zero.

Gas entrainment in the flow system was confirmed in several tests. The injector cavity was observed through window ports, and a dispersion of small bubbles was noted. Similar behavior in a chugging combustor was noted in reference 7. Although quantitative measurements from these observations were not possible, it may be concluded that gas entrainment modified the elasticity of the flow system. Therefore, the expected values of interaction index are less than those shown in figure 16, which assume no gas entrainment. The obvious conclusion is that the interaction index for these combustors exhibits a dispersion of values about a mean level of less than 0.25 and probably near zero.

Time lag. - Time lag is relatively insensitive to the specific parametric values used to satisfy analytical solutions for each test condition. This insensitivity is shown in figure 17, where time lag is presented as a function of combustor pressure for the condition of interaction index equal to zero and also for compressibility equal to that for liquid oxygen. Values are somewhat larger when the index is zero. Although a decrease in time lag with an increase in pressure appears to be a characteristic property of each configuration, the dispersion about a mean variation with pressure is relatively large. Apparently, a unique time lag and pressure relation cannot be used to characterize these configurations.

A variation in time lag with several parameters may be expected. The time lag represents the average time interval between propellant injection and complete chemical conversion. The time required for propellant atomization is included in this time interval. In this study with parallel-jet injection methods, the jet-breakup, or atomization, time is a substantial portion of the total time lag. Parameters affecting jet-breakup time, therefore, must be included in any correlation of time-lag variations.

Although a precise value of time lag cannot be established for each test condition, the values shown in figure 17 exhibit trends that may be related to changes in jet-breakup time. A degree of consistency exists when time lag is assumed to be equal to the summation of a jet-breakup time, vaporization time, and a gas-phase-mixing time. When the mean vaporization and mixing times are approximated by the theoretical combustion gas

residence time  $\theta_g$ , jet-breakup time is given by  $\tau - \theta_g$ . In the subsequent discussion, changes in the value of  $\tau - \theta_g$  are compared with the characteristics of a jet-breakup process. The comparison shows a relation between changes in stability and changes in one mechanism within the overall combustion process.

## EVALUATION OF JET-BREAKUP TIME

### Breakup Processes

Jet breakup has been studied by various investigators (refs. 8 to 10) who showed that breakup in the concurrent flow of a gas and a liquid is related to both the velocity of the liquid jet and the relative velocity between gas and liquid. In general, breakup time in the turbulent flow region decreases with an increase in jet velocity and in relative velocity, where the increased relative velocity is larger at high gas pressures. The effect of jet velocity on breakup time varies with changes in the jet-formation process. The jet may fill the exit orifice, partially separate from the sidewalls of the orifice, or flow completely free of the sidewalls. Partial separation is analogous to cavitation collapse and reduces breakup time relative to breakup when the jet is flowing freely or full. Partial separation and flowing full exhibit higher flow coefficients than that exhibited by flowing free because of changes in effective flow area. Increasing the orifice length of a free-flowing configuration initially causes a transition to partial separation and finally to flowing full. Changes in the liquid cross velocity at the orifice inlet affect the conditions at which these transitions occur.

These qualitative properties of jet breakup will be used to interpret changes in time lag caused by probable changes in jet-breakup time. By this interpretation, the stability characteristics of the various configurations will be related to the jet-breakup process, where breakup is assumed to be controlled by flow conditions prior to any significant burning of propellants.

### Effect of Combustor Configuration Variables on Breakup Time

The properties of each configuration at a combustor pressure of 350 pounds per square inch absolute along the stability boundary are tabulated and compared with those for the reference combustor. Parameters used to characterize jet breakup are the oxygen jet velocity  $U_O$ , the injector orifice discharge coefficient  $C_{Di}$ , and the relative velocity term  $\rho_g/g(U_H - U_O)^2$  expressed as a dynamic pressure. Oxygen jet velocity is the computed value based on mass flow rate and orifice exit area. Hydrogen velocity is

the concurrent flow velocity surrounding the oxygen jet, computed from the mass flow rate and from the combustor cross-sectional area at inlet temperature conditions. The term  $\tau - \theta_g$  is used to indicate the apparent jet-breakup time, as previously discussed. Time-lag values obtained from solutions for an interaction index of zero are used, although the comparison is not dependent on the values of this specific solution.

Characteristic length of combustor:

Configuration variable, $L^*$	System parameter						Jet-breakup time
	$U_O$	$C_{Di}$	$U_H$	$(\rho_g/g)(U_H - U_O)^2$	$\theta_g$	$\tau$	$\tau - \theta_g$
81	16.5	0.505	52.8	4.45	0.0025	0.0189	0.0164
156 (reference)	14.7	.505	45.5	3.21	.0044	.0228	.0184
224	14.2	.505	47.3	3.50	.0061	.0243	.0182

The changes in jet-breakup time  $\tau - \theta_g$ , although small, show a decrease with an increase in jet velocity and dynamic pressure; this behavior is expected for a jet-breakup process. However, the change in vaporization and mixing times  $\theta_g$  appears to cause a larger change in time lag and presumably in stability than that caused by the change in jet-breakup time. The constant discharge coefficient  $C_{Di}$  implies that no change in jet formation process is encountered.

Length to diameter ratio of injector orifice:

Configuration variable, $L/D$	System parameter						Jet-breakup time
	$U_O$	$C_{Di}$	$U_H$	$(\rho_g/g)(U_H - U_O)^2$	$\theta_g$	$\tau$	$\tau - \theta_g$
1.56 (reference)	14.7	0.505	45.5	3.21	0.0044	0.0228	0.0184
3.90	13.1	.620	53.1	5.40	.0039	.0185	.0146
6.25	13.2	.675	53.6	5.51	.0042	.0185	.0143

An increase in orifice  $L/D$  decreased the jet-breakup time. The decrease is not consistent with the behavior expected for the decrease in jet velocity, or for the increase in dynamic pressure. A change in jet formation, however, is probable, as indicated by the increase in the discharge coefficient. This increase is characteristic of a jet that flows freely at a small  $L/D$  but is only partially separated from the orifice sidewalls at a larger  $L/D$ . The more turbulent jet formation with partial separation is a probable

cause of the decrease in breakup time. An examination of all the data showed that this turbulent jet was less sensitive to changes in dynamic pressure than a free jet.

Number of jets:

Configuration variable, number of jets	System parameter						Jet-breakup time
	$U_O$	$C_{Di}$	$U_H$	$(\rho_g/g)(U_H - U_O)^2$	$\theta_g$	$\tau$	$\tau - \theta_g$
20	26.2	0.509	59	3.64	0.0042	0.0181	0.0139
40 (reference)	14.7	.505	45.5	3.21	.0044	.0228	.0184
60	11.1	.568	37.1	2.30	.0048	.0191	.0143

Jet-breakup time is smaller for both the 20- and the 60-jet configurations than for the 40-jet reference configuration. The decrease in breakup time for the 20-jet configuration appears consistent with the increase in jet velocity. The decrease for the 60-jet configuration, however, must be attributed to a change in jet formation, as implied by the increase in the discharge coefficient. The relative cross velocity is higher for the 60-jet configuration than for a configuration with fewer jets and may have promoted partial flow separation from the orifice sidewalls.

Flow-system volume:

Configuration variable, flow-system volume	System parameter						Jet-breakup time
	$U_O$	$C_{Di}$	$U_H$	$(\rho_g/g)(U_H - U_O)^2$	$\theta_g$	$\tau$	$\tau - \theta_g$
Reference	14.7	0.505	45.5	3.21	0.0044	0.0228	0.0184
Large injector cavity	12.5	.680	58.2	7.06	.0040	.0181	.0141
Extended manifold	15.1	.505	44.7	2.96	.0050	.0242	.0192

The small increase in breakup time for the extended manifold configuration is in agreement with the small changes in the velocity and dynamic pressure parameters. The decrease in breakup time for the large injector cavity configuration is significant; it may be partially attributed to the large increase in dynamic pressure. However, the increase in discharge coefficient indicates a condition of partial flow separation, which would also decrease breakup time. Lower cross velocities with the large cavity could cause such a jet formation change.

Diameter of upstream orifice:

Configuration variable, diameter of upstream orifice	System parameter						Jet- breakup time
	$U_O$	$C_{Di}$	$U_H$	$(\rho_g/g)(U_H - U_O)^2$	$\theta_g$	$\tau$	$\tau - \theta_g$
0.052	9.5	0.505	110.0	34.2	0.0040	0.0150	0.0110
.070 (reference)	14.7	.505	45.5	3.21	.0044	.0228	.0184

Flow conditions at the stability boundary were significantly different for the small upstream orifice from those for the reference configuration. The order-of-magnitude increase in dynamic pressure apparently reduced the jet-breakup time even though the decrease in jet velocity would cause the opposite effect. Jet-formation process appears unaffected.

Splash plate:

A numerical comparison between the splash-plate configuration and the reference configurations is not possible because the solutions for a negative interaction index required for the splash plate were not evaluated.

### Effect of Jet Breakup on Interaction Index

The interaction index  $n$  is a measure of the pressure sensitivity of the combustion process; it is also a measure of the perturbation in time lag caused by a perturbation in combustor pressure. It has been previously established that a value of  $n$  at or near zero is the probable average value for these configurations. Pressure oscillations, therefore, should cause small variations in jet-breakup time, since delay time and breakup time are closely related. The qualitative properties of jet breakup do not clearly indicate a small value of  $n$ . However, an increase in combustor pressure would decrease jet velocity and increase delay time (negative values of  $n$ ), whereas an increase in pressure would also increase the dynamic pressure and decrease breakup time (positive values of  $n$ ). The relative importance of these two effects would require a quantitative description of the jet-breakup process.

In the case of the splash-plate configuration, where a negative interaction index is clearly established, a decrease in time lag with pressure should be evident. Here, jet

impingement is on a solid body, and breakup or atomization time may be more dependent on jet velocity than it is for the nonimpinging jets. This would reduce the effectiveness of the dynamic pressure on atomization and cause the negative  $n$  characteristic of a jet-velocity increase to predominate.

## AVERAGE FUNCTIONAL VARIATION OF TIME LAG

The jet formation of the reference configuration is believed to be that of a jet flowing freely of the orifice sidewalls. This jet form was exhibited by several configurations that provided stability data over a broad range of operating conditions. These data were used to formulate a relation for jet breakup.

In formulating the relation, a basic breakup time was assumed to be established by jet turbulence and other flow disturbances caused by flow through an orifice. This basic breakup time was reduced by the dynamic pressure forces acting on the jet during the period of breakup. The relation formulated on the basis of such a model is

$$\tau_j = \frac{0.2}{U_O^{0.75}} - \tau_j \left[ 0.1 \frac{\rho_g}{g} (U_H - U_O)^2 \right]$$

or

$$\tau_j = \frac{\frac{0.2}{U_O^{0.75}}}{1 + 0.1 \frac{\rho_g}{g} (U_H - U_O)^2}$$

With the aid of this equation for jet-breakup time and the relation  $\tau = \tau_j + \theta_g$ , values of time lag are defined for all operating conditions of the reference combustor configuration. Figure 18 shows time lags for the range of conditions considered in this study. In general, time lag varies with hydrogen flow rate and is relatively constant with variations in oxygen flow rate.

Figure 18 displays the time lags that characterize the combustion process for a range of operational conditions. The specific values that apply to the condition of neutral stability depend on the interaction of many stability parameters and analytically involve a complex interactive procedure where boundary conditions continually change until convergence at neutral stability is obtained. Such solutions are possible; however, greater precision is needed in describing time-lag variations with operating conditions if these

variations are to be useful in analytically modeling the effect of system variables on stability observed in this study.

## SUMMARY OF RESULTS

Chugging instability limits were experimentally established in a parametric study of a small-scale combustor system that used parallel-jet injection of liquid oxygen into diffusely injected gaseous hydrogen. System stability was experimentally characterized by the range of the stable operating region and by the inherent stability related to the oxygen flow-system drop at the stability boundary. An analytical model of the experimental combustor system was developed. With this model the configurations were characterized by a time lag (delay time between injection and burning) and by an interaction index (sensitivity of combustion to pressure oscillations).

In general, no predictable trends in the variations of interaction index were noted. The average value for all tests was less than 0.25. Time lag appeared to vary systematically and was related to the sum of a liquid jet-breakup time and a vaporization and mixing time, with the contribution of breakup time being predominant. Breakup time was dependent on the jet-formation process (flowing freely or attached to the orifice sidewalls) and on the aerodynamic forces imposed by the combustor gases. A relation for breakup time was formulated for a jet flowing freely of the sidewalls.

The principal effects of specific combustor-system variables on stability are summarized as follows:

1. Characteristic length: An increase in characteristic length increased the range of stable operation, inherent stability, time lag (vaporization and mixing), and combustor performance. Jet flow remained free of the orifice sidewalls.
2. Injector orifice length to diameter ratio: An increase in orifice length to diameter ratio increased the range of stable operation and the inherent stability. Jet flow apparently attached to the sidewalls with an increase in length to diameter ratio causing a decrease in time lag (breakup time) and an increase in flow-system pressure drop.
3. Number of jets: An increase in the number of injector orifices, or jets, decreased the range of stable operation and inherent stability. A large number of jets affected the jet-formation process and decreased the time lag (jet-breakup time).
4. Flow-system volume: Increasing the flow-system volume by extending the injector manifold decreased the range of stable operation and the inherent stability, whereas increasing the size of the injector cavity had the inverse effect. Gas entrainment due to heat transfer and/or local cavitation was experimentally and analytically identified within the combustor system and may have contributed to these effects. Time lag (jet-breakup time) decreased with enlargement of the injector cavity, and jet flow exhibited a condition

of partial separation from the orifice sidewalls.

5. Upstream orifice: Increasing the flow-system pressure drop by inserting a small orifice in the supply line increased the range of stable operation but decreased the inherent stability. Time lag (jet-breakup time) decreased in a predictable manner for a free-flowing jet.

6. Splash plate: Impingement of oxygen jets on a splash plate increased the range of stable operation and the inherent stability. Negative values of the interaction index were established for the splash-plate configuration; however, time-lag values were not evaluated analytically.

Lewis Research Center,  
National Aeronautics and Space Administration,  
Cleveland, Ohio, November 17, 1966,  
126-31-06-02-22.

## REFERENCES

1. Crocco, Luigi; and Cheng, Sin-I: Theory of Combustion Instability in Liquid Propellant Rocket Motors. Butterworths Scientific Publications, 1956.
2. Summerfield, Martin: A Theory of Unstable Combustion in Liquid Propellant Rocket Systems. ARS J., vol. 21, no. 5, Sept. 1951, pp. 108-114.
3. Barrère, M.; and Moutet, A.: Low-Frequency Combustion Instability in Bipropellant Rocket Motors - Experimental Study. Jet Propulsion, vol. 26, no. 1, Jan. 1956, pp. 9-19.
4. Gunder, D. F.; and Friant, D. R.: Stability of Flow in a Rocket Motor. J. Appl. Mech., vol. 17, no. 3, Sept. 1950, pp. 327-333.
5. Crocco, L.: Aspects of Combustion Stability in Liquid Propellant Rocket Motors. ARS J., vol. 21, no. 6, Nov. 1951, pp. 163-178.
6. Minorsky, Nicholas: Self-Excited Oscillations in Dynamical Systems Possessing Retarded Actions. J. Appl. Mech., vol. 9, no. 2, June 1942, pp. A65-A71.
7. Conrad, E. William; Hannum, Ned P.; and Bloomer, Harry E.: Photographic Study of Liquid-Oxygen Boiling and Gas Injection in the Injector of a Chugging Rocket Engine. NASA TM X-948, 1964.
8. Miesse, C. C.: Correlation of Experimental Data on the Disintegration of Liquid Jets. Ind. Eng. Chem., vol. 47, 1955, pp. 1690-1701.

9. Eisenklam, P.; and Hooper, P. C.: The Flow Characteristics of Laminar and Turbulent Jets of Liquid. Rep. No. JRL 42, Imperial College of Science and Tech., London, Sept. 1958.
10. Lyishevski, A. S.: On the Influence of Turbulence Upon the Disintegration of Liquid Jets; Politekhnikheskiy Institute, Novocherkassk, vol. 39, no. 53, 1957, pp. 81-86.

TABLE I. - ANALYTICAL SOLUTIONS

Operating parameter						Interaction index, n														
Mass flow rate, lb/sec		Combus-tor pres-sure, P <sub>c</sub> , psi	Charac-teristic ex-haust velocity, c*, ft/sec	Pres-sure-drop param-eter of in-jector orifice, P	Fre-quen-cy, f, cps	Mean gas resi-dence time in combus-tor, θ <sub>g</sub> , msec	0		0.1		0.2		0.3		0.4		0.5		0.6	
							Liquid compress-ibility, ε, psi <sup>-1</sup>	Time lag, τ, msec	Liquid compress-ibility, ε, psi <sup>-1</sup>	Time lag, τ, msec	Liquid compress-ibility, ε, psi <sup>-1</sup>	Time lag, τ, msec	Liquid compress-ibility, ε, psi <sup>-1</sup>	Time lag, τ, msec	Liquid compress-ibility, ε, psi <sup>-1</sup>	Time lag, τ, msec	Liquid compress-ibility, ε, psi <sup>-1</sup>	Time lag, τ, msec	Liquid compress-ibility, ε, psi <sup>-1</sup>	Time lag, τ, msec
Reference configuration <sup>a</sup> (Y = 0)																				
0.323	0.088	288	6770	29.4	20	4.60	62.9×10 <sup>-6</sup>	28.1	51.1×10 <sup>-6</sup>	26.4	35.8×10 <sup>-6</sup>	24.2	0.815×10 <sup>-6</sup>	19.4	-----	-----	-----	-----	-----	-----
.411	.129	400	7170	25.6	28	4.30	46.6	19.9	40.5	18.5	33.5	17.7	24.4	16.2	9.50×10 <sup>-6</sup>	13.8	-----	-----	-----	-----
.463	.171	487	7440	24.3	34	4.09	38.0	16.2	33.9	15.5	29.2	14.6	23.6	13.6	16.4	12.3	0.130×10 <sup>-6</sup>	9.86	-----	-----
.497	.207	538	7390	23.6	37	4.06	35.1	14.8	31.8	14.2	27.9	13.4	23.5	12.6	18.1	11.5	10.3	10.1	-----	-----
Reference configuration <sup>a</sup> (Y = 1)																				
0.323	0.088	288	6770	29.4	20	4.60	67.0×10 <sup>-6</sup>	28.5	54.6×10 <sup>-6</sup>	26.8	38.6×10 <sup>-6</sup>	24.6	5.65×10 <sup>-6</sup>	20.0	-----	-----	-----	-----	-----	-----
.411	.129	400	7170	25.6	28	4.30	51.0	20.3	44.4	19.3	36.7	18.1	27.3	16.5	12.1×10 <sup>-6</sup>	14.2	-----	-----	-----	-----
.463	.171	487	7440	24.3	34	4.09	42.2	16.6	37.7	15.9	32.6	15.0	26.5	13.9	18.8	12.6	4.16×10 <sup>-6</sup>	10.2	-----	-----
.497	.207	538	7390	23.6	37	4.06	39.6	15.2	35.8	14.5	31.3	13.8	26.5	12.9	20.7	11.8	12.5	10.4	-----	-----
Characteristic length, L*, 81 in. (Y = 0)																				
0.354	0.088	255	5580	21.6	24	2.92	64.5×10 <sup>-6</sup>	24.9	54.2×10 <sup>-6</sup>	23.6	41.2×10 <sup>-6</sup>	22.0	21.8×10 <sup>-6</sup>	19.5	-----	-----	-----	-----	-----	-----
.422	.129	359	6310	21.6	34	2.54	39.6	17.2	33.8	16.3	26.9	15.3	17.3	13.8	-----	-----	-----	-----	-----	-----
.469	.172	436	6580	21.4	40	2.40	31.5	14.4	27.2	13.8	22.2	12.9	15.6	11.7	2.53×10 <sup>-6</sup>	9.62	-----	-----	-----	-----
.502	.213	494	6680	21.1	46	2.33	26.6	12.4	23.3	11.8	19.4	11.1	14.6	10.2	7.30	8.91	-----	-----	-----	-----
Characteristic length, L*, 224 in. (Y = 0)																				
0.284	0.088	275	7180	36.2	19	6.18	61.5×10 <sup>-6</sup>	27.9	49.1×10 <sup>-6</sup>	26.1	32.2×10 <sup>-6</sup>	23.6	-----	-----	-----	-----	-----	-----	-----	-----
.393	.129	392	7310	27.2	25	6.05	56.8	21.7	50.7	20.7	43.7	19.6	35.8×10 <sup>-6</sup>	18.2	25.2×10 <sup>-6</sup>	16.5	5.3×10 <sup>-6</sup>	13.6	-----	-----
.442	.172	472	7460	25.9	30	3.94	39.2	18.6	34.1	17.7	27.9	16.5	19.9	15.1	5.41	12.6	-----	-----	-----	-----
.455	.212	518	7550	27.3	33	5.68	42.1	16.1	38.6	15.4	34.8	14.7	30.7	13.9	25.9	12.9	20.3×10 <sup>-6</sup>	11.9	11.6×10 <sup>-6</sup>	10.5
Length to diameter ratio of injector orifice, L/D, 3.90 (μ = 77.44, Y = 0)																				
0.260	0.088	259	7420	66.4	24	4.02	37.4×10 <sup>-6</sup>	21.5	23.9×10 <sup>-6</sup>	19.6	-----	-----	-----	-----	-----	-----	-----	-----	-----	-----
.334	.129	355	7640	55.5	30	3.86	35.1	17.8	28.4	16.7	19.7×10 <sup>-6</sup>	15.2	5.2×10 <sup>-6</sup>	12.4	-----	-----	-----	-----	-----	-----
.385	.172	448	8020	52.7	36	3.63	28.9	14.8	24.5	14.0	19.1	13.0	11.5	11.6	-----	-----	-----	-----	-----	-----
.423	.211	512	8060	50.0	40	3.59	26.6	13.3	23.2	12.6	19.2	11.8	14.2	10.8	6.15×10 <sup>-6</sup>	9.35	-----	-----	-----	-----

Length to diameter ratio of injector orifice, L/D, 6.25 ( $\omega = 85.25$ ,  $Y = 0$ )

0.261	0.088	253	7000	71.1	26	4.41	$39.9 \times 10^{-6}$	19.8	$29.5 \times 10^{-6}$	18.3	$13.1 \times 10^{-6}$	16.0	-----	-----	-----	-----	-----	-----	-----	-----
.339	.129	358	7390	59.7	30	4.13	37.0	17.8	30.6	16.7	22.8	15.4	$10.5 \times 10^{-6}$	13.4	-----	-----	-----	-----	-----	-----
.391	.173	436	7460	54.5	34	4.04	33.5	15.8	28.9	15.0	23.7	14.0	16.8	12.7	$4.6 \times 10^{-6}$	10.7	-----	-----	-----	-----
.398	.217	473	7430	57.0	37	4.00	29.5	14.3	25.7	13.6	21.3	12.7	15.7	11.6	6.8	10.0	-----	-----	-----	-----

20 Injector orifices ( $A_1 = 0.02515$ ,  $\omega = 11.834$ ,  $Y = 0$ )

0.286	0.088	269	6970	9.03	25	4.67	$52.4 \times 10^{-6}$	20.9	$42.1 \times 10^{-6}$	19.7	$29.5 \times 10^{-6}$	18.1	$5.68 \times 10^{-6}$	15.2	-----	-----	-----	-----	-----	-----
.318	.129	329	7120	8.89	28	4.23	43.0	18.6	35.1	17.6	25.1	16.2	8.50	14.0	-----	-----	-----	-----	-----	-----
.366	.171	402	7250	8.24	32	4.11	38.6	16.3	32.6	15.5	25.8	14.5	17.1	13.2	-----	-----	-----	-----	-----	-----
.413	.214	474	7320	7.57	38	4.04	34.1	13.6	30.1	13.0	25.7	12.3	20.5	11.5	$13.9 \times 10^{-6}$	10.4	$1.05 \times 10^{-6}$	8.34	-----	-----

60 Injector orifices ( $A_1 = 0.07545$ ,  $\omega = 135.46$ ,  $Y = 0$ )

0.416	0.089	352	6720	62.4	30	4.76	$53.5 \times 10^{-6}$	18.7	$48.5 \times 10^{-6}$	17.9	$42.4 \times 10^{-6}$	16.9	$35.7 \times 10^{-6}$	15.8	$27.3 \times 10^{-6}$	14.4	$14.7 \times 10^{-6}$	12.6	-----	-----
.473	.130	445	7120	60.5	36	4.42	42.1	15.4	38.6	14.8	34.8	14.1	30.2	13.2	25.0	12.3	18.3	11.1	$7.25 \times 10^{-6}$	9.38
.572	.172	568	7350	53.1	42	4.24	36.0	13.2	33.8	12.7	31.1	12.2	28.1	11.5	24.7	10.8	20.9	10.0	16.1	9.12

Large injector cavity ( $\omega = 93.142$ ,  $A = 0.197$ ,  $Y = 0$ )

0.211	0.086	231	7510	108	23	4.01	$3.68 \times 10^{-6}$	18.3	-----	-----	-----	-----	-----	-----	-----	-----	-----	-----	-----	-----
.293	.128	322	7390	78.2	28	4.06	22.9	18.4	$16.8 \times 10^{-6}$	17.0	$6.73 \times 10^{-6}$	14.7	-----	-----	-----	-----	-----	-----	-----	-----
.360	.170	418	7610	67.4	32	3.91	22.1	16.6	18.2	15.6	13.3	14.3	$5.1 \times 10^{-6}$	12.3	-----	-----	-----	-----	-----	-----
.373	.211	473	7810	71.0	34	3.77	18.8	15.4	15.3	14.4	10.8	13.2	2.25	11.0	-----	-----	-----	-----	-----	-----

Extended manifold ( $L = 70.40$ ,  $Y = 0$ )

0.344	0.088	298	6530	26.9	20	4.94	$18.9 \times 10^{-6}$	27.1	$15.8 \times 10^{-6}$	25.7	$12.0 \times 10^{-6}$	23.8	$6.12 \times 10^{-6}$	21.0	-----	-----	-----	-----	-----	-----
.423	.131	412	7040	24.7	27	4.51	13.2	19.7	11.6	18.8	9.62	17.6	7.12	16.2	$3.32 \times 10^{-6}$	14.2	-----	-----	-----	-----
.473	.172	493	7220	23.7	31	4.32	11.1	17.0	9.88	16.3	8.46	15.4	6.74	14.2	4.43	12.8	$0.55 \times 10^{-6}$	10.3	-----	-----
.510	.216	559	7270	23.3	35	4.23	9.60	14.9	8.65	14.2	7.60	13.5	6.35	12.6	4.77	11.6	2.48	10.2	-----	-----

Diameter of upstream orifice, 0.052 in. ( $A_u = 0.00212$ ,  $\omega = 176.23$ ,  $Y = 0$ )

0.164	0.088	174	6930	66.9	19	4.13	$60.0 \times 10^{-6}$	32.3	$51.8 \times 10^{-6}$	30.8	$42.1 \times 10^{-6}$	28.9	$29.7 \times 10^{-6}$	26.3	-----	-----	-----	-----	-----	-----
.181	.130	219	7060	70.2	22	3.98	46.3	27.5	40.2	26.2	32.9	24.6	23.8	22.5	$6.78 \times 10^{-6}$	18.6	-----	-----	-----	-----
.199	.173	266	7170	70.0	25	3.88	37.7	24.0	33.2	22.9	27.8	21.5	21.0	19.8	10.5	17.1	-----	-----	-----	-----
.219	.215	304	7030	66.7	36	3.94	28.5	16.0	26.1	15.4	23.4	14.6	20.2	13.7	16.5	12.7	$11.5 \times 10^{-6}$	11.3	$0.66 \times 10^{-6}$	8.89

Splash plate ( $Y = 0$ )

0.120	0.173	223	7460	159	19	3.73	-----	>22.1	-----	-----	-----	-----	-----	-----	-----	-----	-----	-----	-----	-----
.192	.216	315	7560	89.5	20	3.71	-----	>21.1	-----	-----	-----	-----	-----	-----	-----	-----	-----	-----	-----	-----

<sup>a</sup>Length to diameter ratio of injector orifice, 1.56; 40 jets; length of flow-system supply line, 22.4 in.; area of upstream orifice, 0.00384 in.<sup>2</sup>; area of injector orifice, 0.0503 in.<sup>2</sup>; characteristic length of combustor, 156 in.; resistance parameter of flow system, 47.348; effective area of flow system supply line, 0.14 in.<sup>2</sup>.

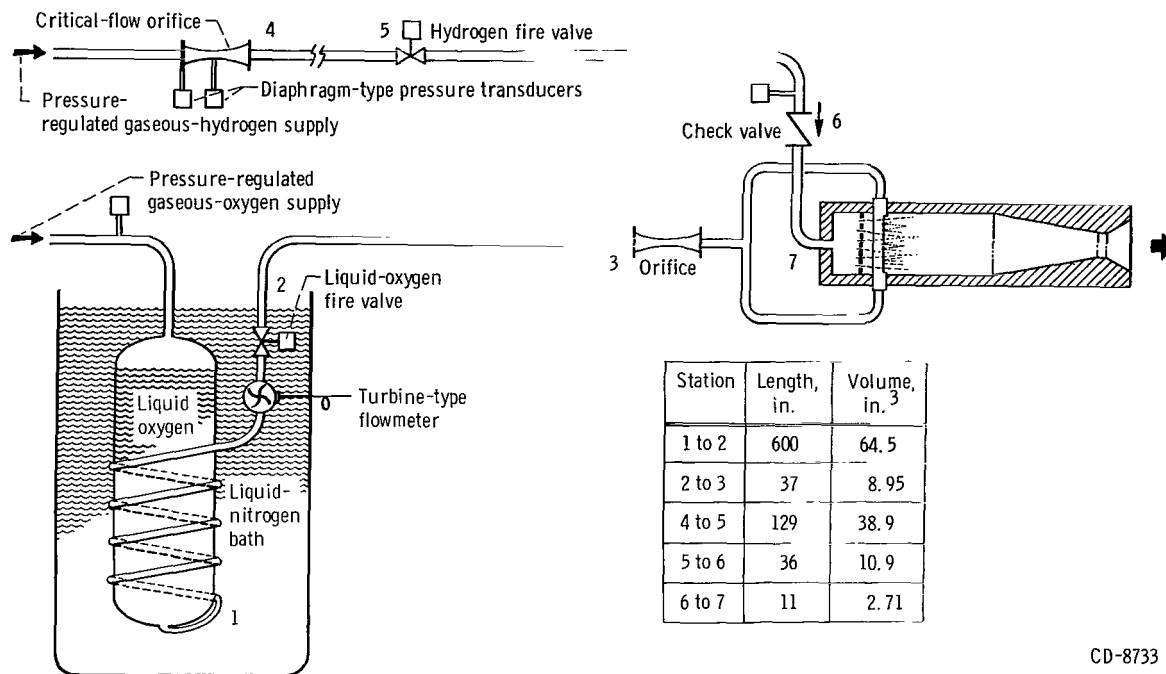


Figure 1. - Schematic diagram of combustor flow system.

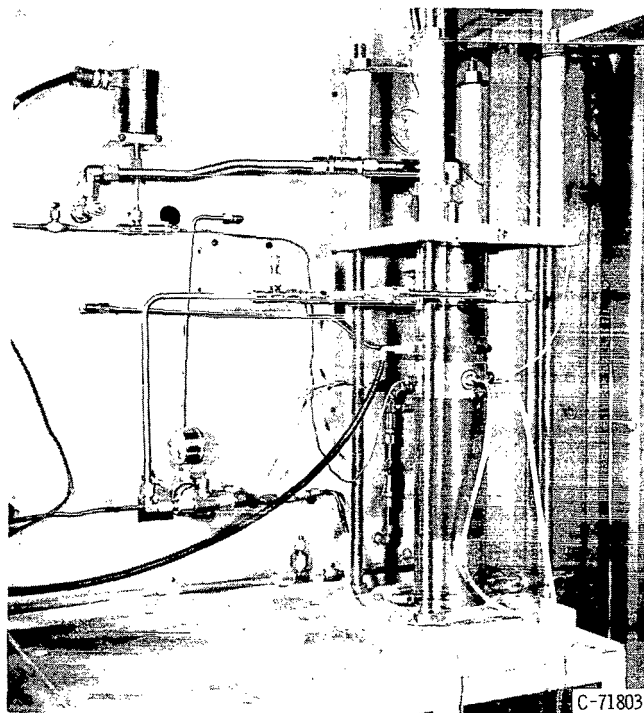
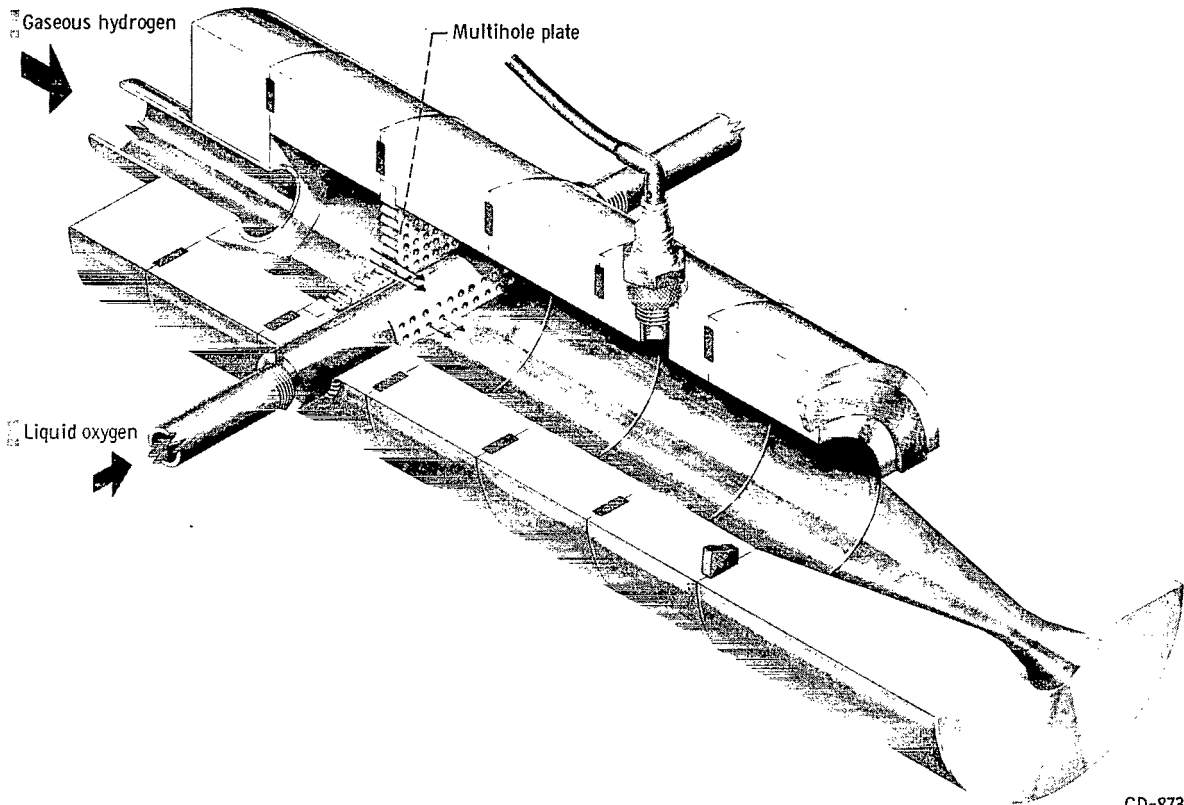
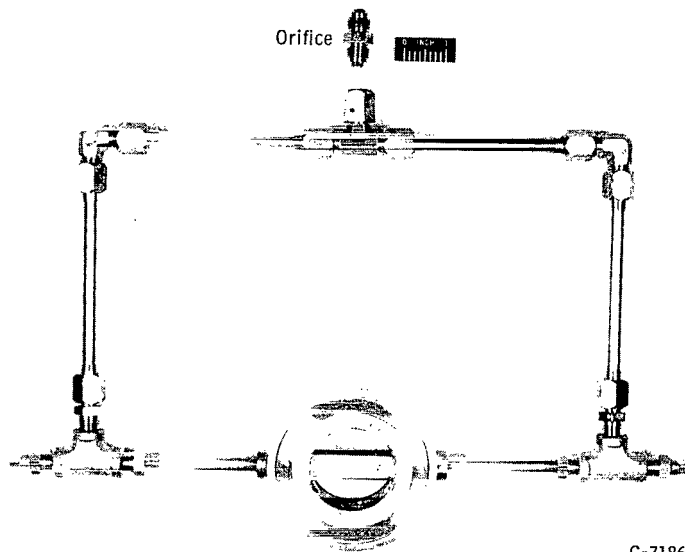


Figure 2. - Test cell installation of experimental combustor.



CD-8732

Figure 3. - Gaseous-hydrogen - liquid-oxygen combustor. Chamber diameter, 2 inches; mean nozzle diameter, 0.620 inch; axial distance from liquid-oxygen injector to nozzle throat, 9.5 to 23.0 inches (variable).



C-71862

Figure 4. - Liquid-oxygen injector and manifold.

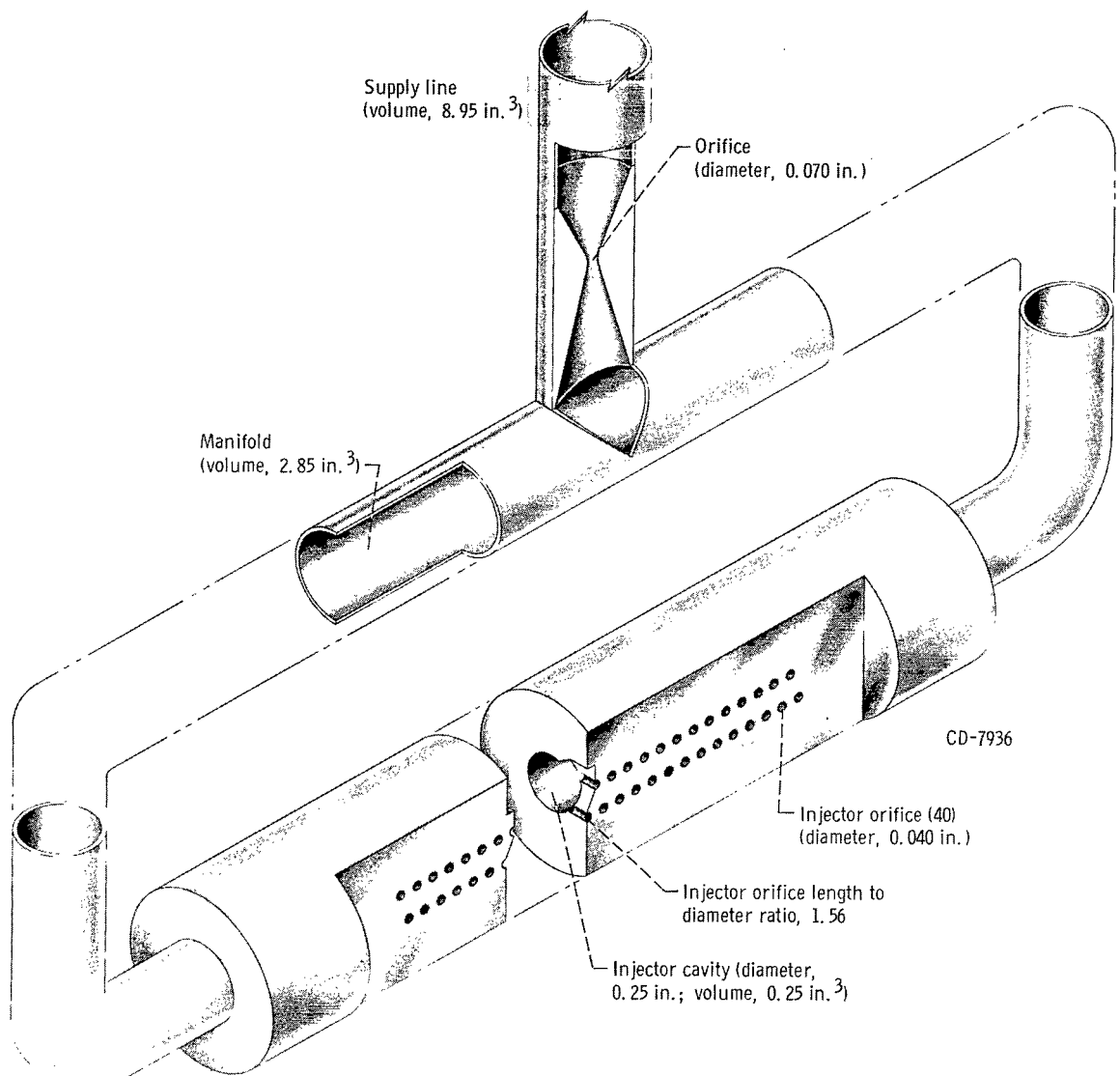
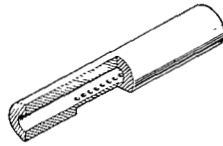
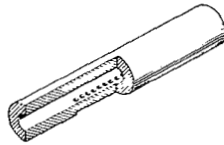


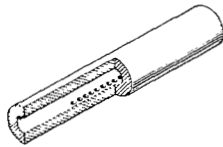
Figure 5. - Reference liquid-oxygen injector and manifold configuration.



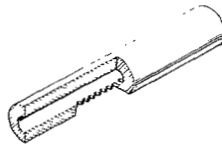
(a) Reference configuration; 40 jets; length to diameter ratio, 1.56; cavity volume, 0.25 cubic inch.



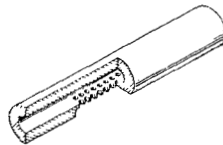
(b) Length to diameter ratio, 3.90.



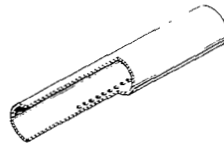
(c) Length to diameter ratio, 6.25.



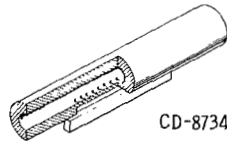
(d) 20 Jets.



(e) 60 Jets.



(f) Cavity volume, 1.56 cubic inches.



(g) Splash plate.

Figure 6. - Liquid-oxygen injector cavity and orifice configurations.

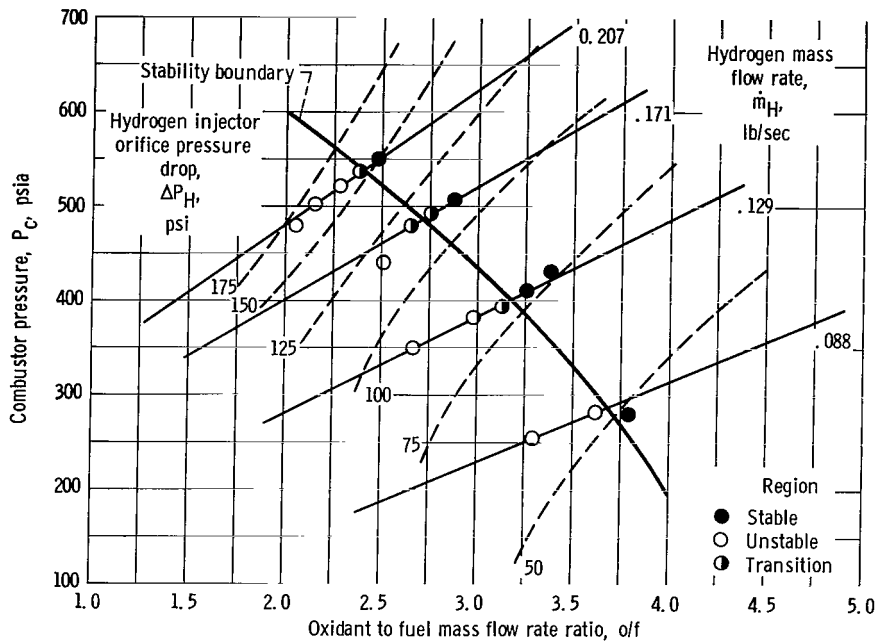


Figure 7. - Chamber pressure as function of oxidant-fuel ratio for reference combustor. 40 Parallel jets; length to diameter ratio of injector orifice, 1.56; characteristic length of combustor, 156 inches; volume of liquid-oxygen cavity, 0.25 cubic inch; diameter of upstream orifice, 0.070 inch.

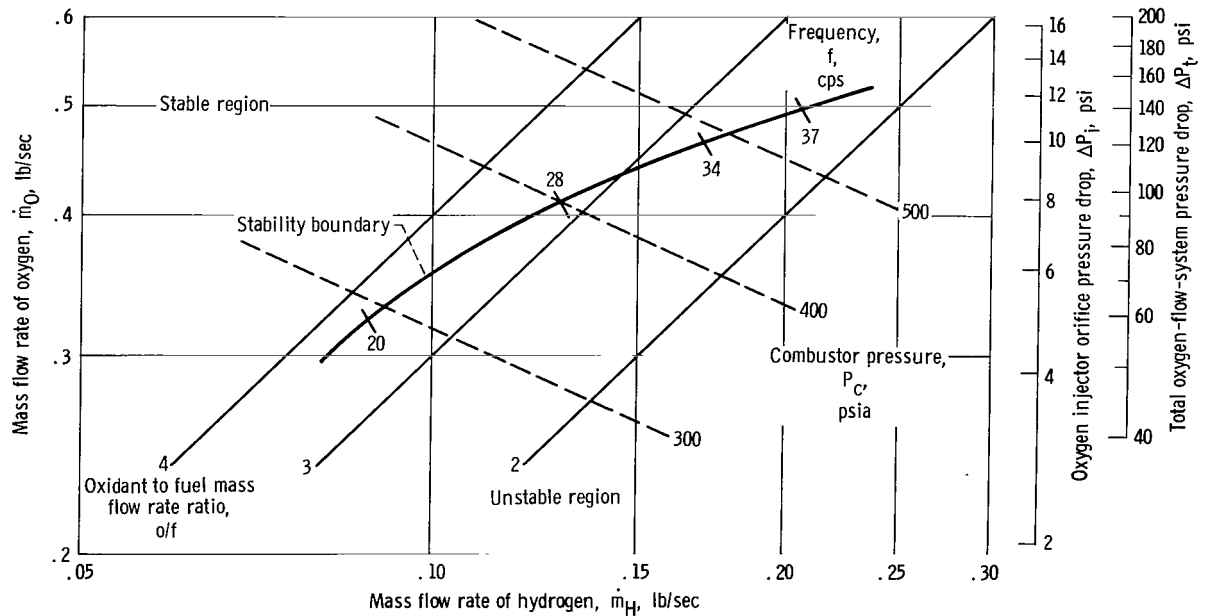


Figure 8. - Composite stability plot of liquid-oxygen weight flow rate as function of gaseous-hydrogen weight flow rate for reference combustor. 40 Parallel jets; length to diameter ratio of injector orifice, 1.56; volume of liquid-oxygen cavity, 0.25 cubic inch; characteristic length of combustor, 156 inches; diameter of upstream orifice, 0.070 inch.

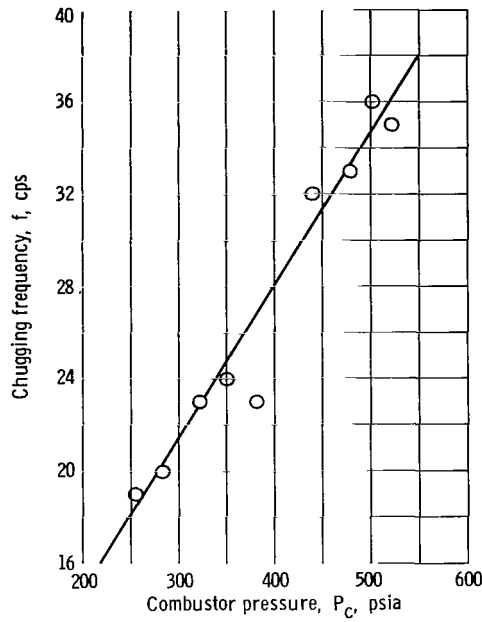


Figure 9. - Chugging frequency as function of chamber pressure. 40 Parallel jets; length to diameter ratio of injector orifice, 1.56; characteristic length of combustor, 156 inches; diameter of upstream orifice, 0.070 inch; volume of liquid-oxygen cavity, 0.25 cubic inch.

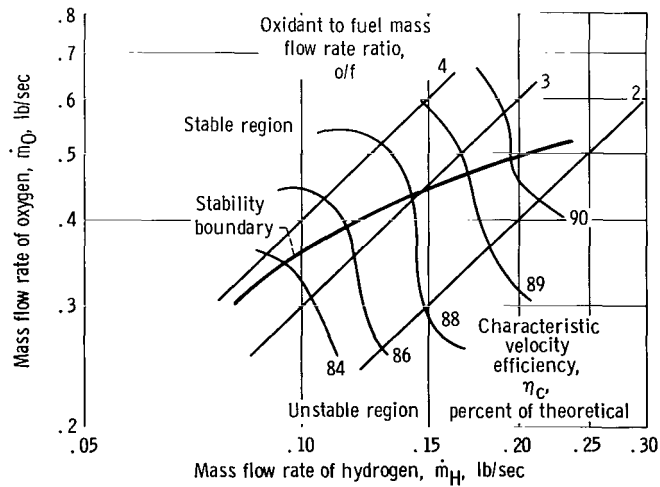


Figure 10. - Reference combustor efficiency map. 40 Parallel jets; length to diameter ratio of injector orifice, 1.56; characteristic length of combustor, 156 inches.

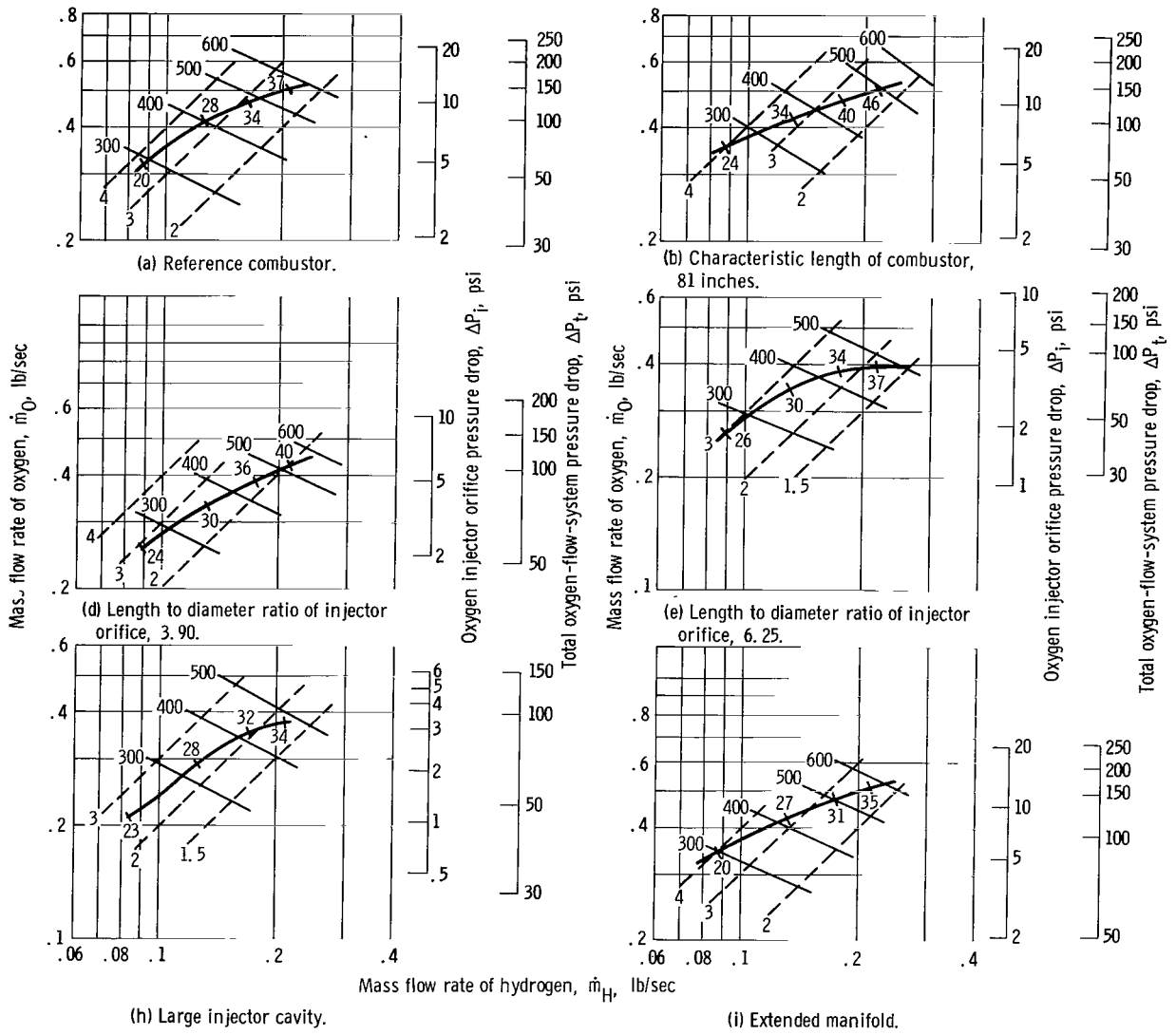
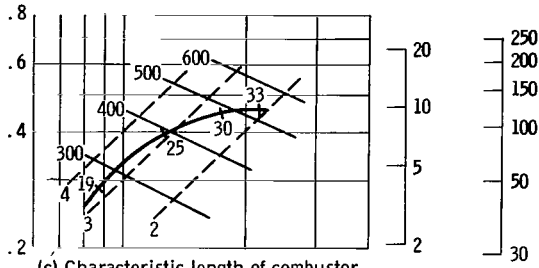
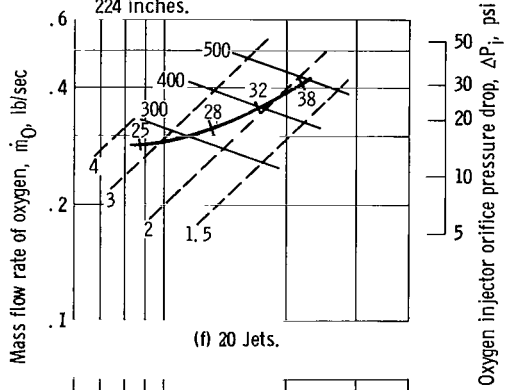


Figure 11. - Combustor--

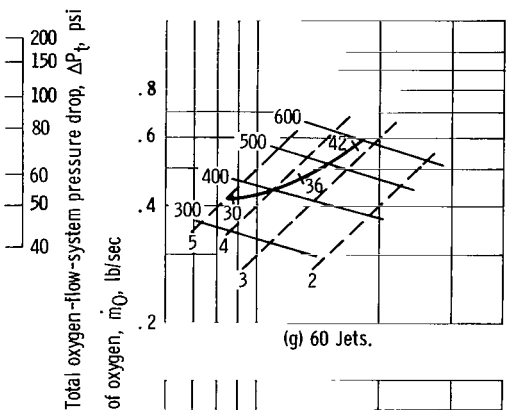


(c) Characteristic length of combustor, 224 inches.

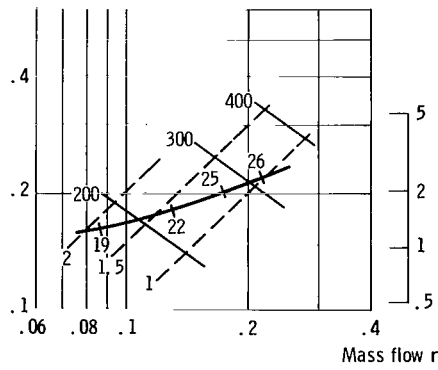
— Combustor pressure, psia  
 - - - Oxidant to fuel weight flow rate ratio  
 — Stability boundary, stable above, unstable below  
 \ Denotes value of oscillatory frequency in cps



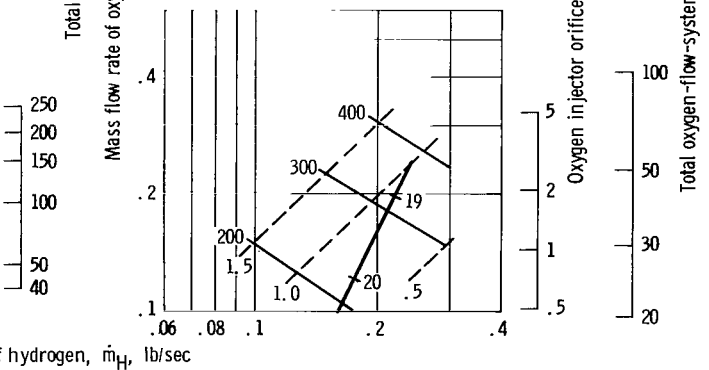
(f) 20 Jets.



(g) 60 Jets.



(j) Diameter of upstream orifice, 0.052 inch.



(k) Splash plate.

performance maps.

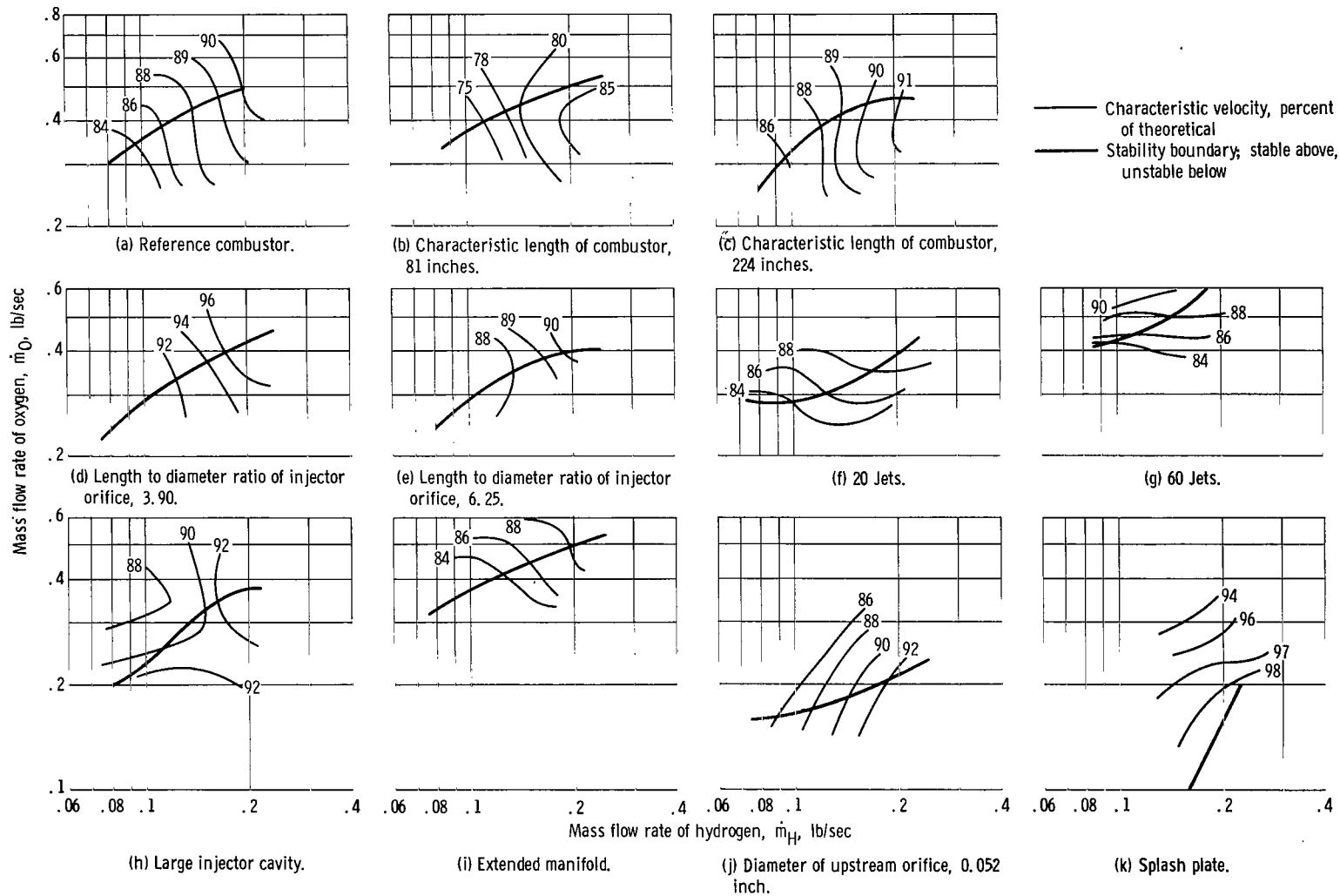


Figure 12. - Combustor efficiency maps.

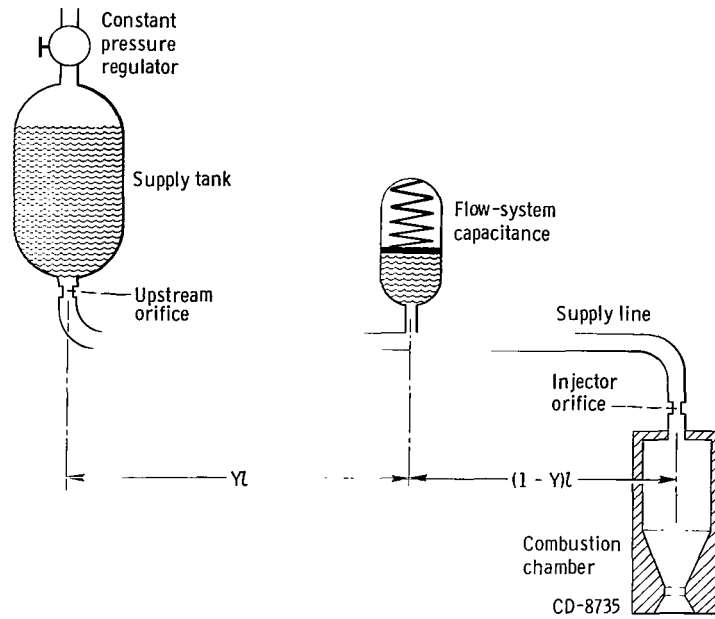


Figure 13. - Schematic diagram of oxygen flow system.

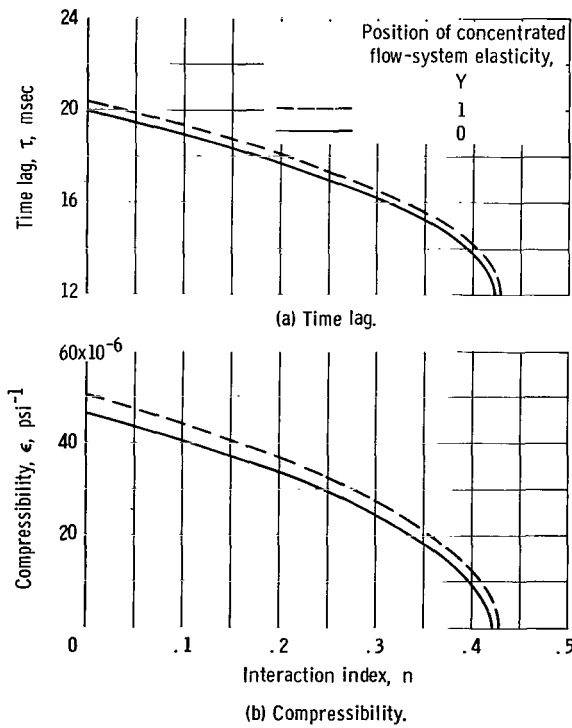


Figure 14. - Range of probable analytical solutions for one operating condition.

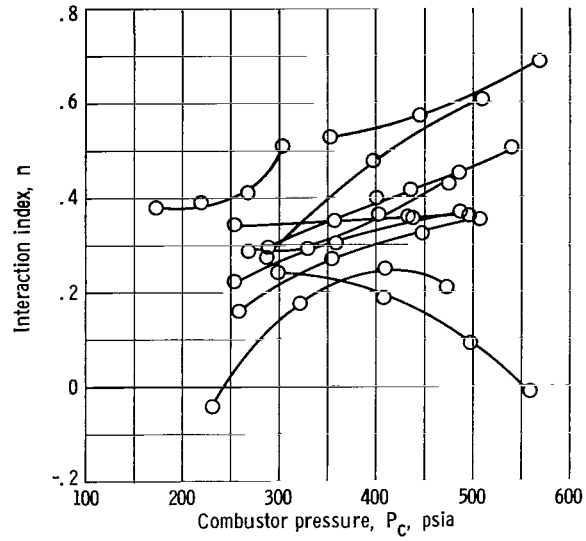


Figure 15. - Relation between interaction index and combustor pressure for liquid compressibility of  $10 \times 10^{-6} \text{ psi}^{-1}$ .

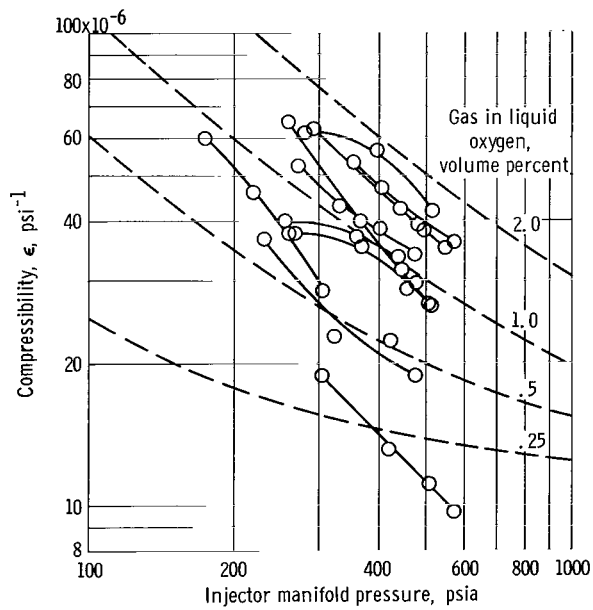


Figure 16. - Liquid compressibility for solutions with interaction index of zero.

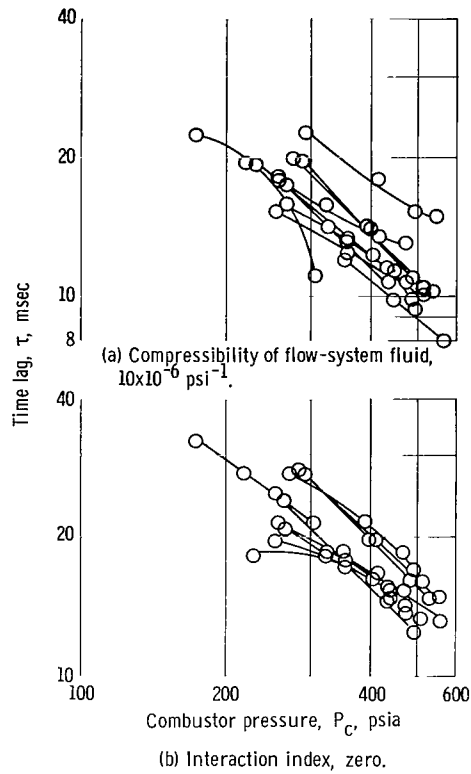


Figure 17. - Time lag solutions for constant compressibility and constant interaction index.

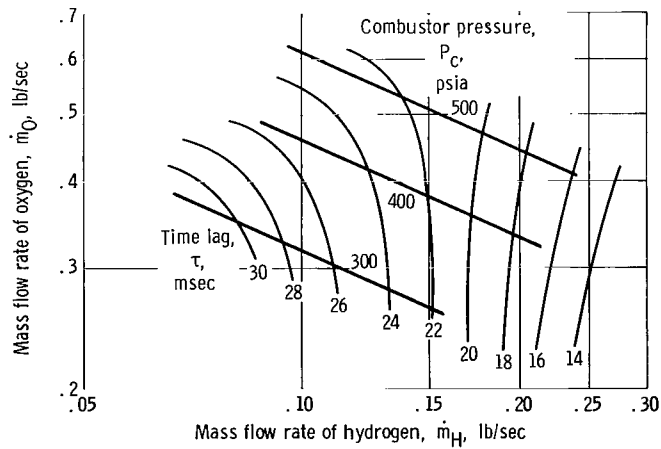


Figure 18. - Time-lag variations for burning rate process controlled by typical jet breakup.

*"The aeronautical and space activities of the United States shall be conducted so as to contribute . . . to the expansion of human knowledge of phenomena in the atmosphere and space. The Administration shall provide for the widest practicable and appropriate dissemination of information concerning its activities and the results thereof."*

—NATIONAL AERONAUTICS AND SPACE ACT OF 1958

## NASA SCIENTIFIC AND TECHNICAL PUBLICATIONS

**TECHNICAL REPORTS:** Scientific and technical information considered important, complete, and a lasting contribution to existing knowledge.

**TECHNICAL NOTES:** Information less broad in scope but nevertheless of importance as a contribution to existing knowledge.

**TECHNICAL MEMORANDUMS:** Information receiving limited distribution because of preliminary data, security classification, or other reasons.

**CONTRACTOR REPORTS:** Scientific and technical information generated under a NASA contract or grant and considered an important contribution to existing knowledge.

**TECHNICAL TRANSLATIONS:** Information published in a foreign language considered to merit NASA distribution in English.

**SPECIAL PUBLICATIONS:** Information derived from or of value to NASA activities. Publications include conference proceedings, monographs, data compilations, handbooks, sourcebooks, and special bibliographies.

**TECHNOLOGY UTILIZATION PUBLICATIONS:** Information on technology used by NASA that may be of particular interest in commercial and other non-aerospace applications. Publications include Tech Briefs, Technology Utilization Reports and Notes, and Technology Surveys.

*Details on the availability of these publications may be obtained from:*

SCIENTIFIC AND TECHNICAL INFORMATION DIVISION  
NATIONAL AERONAUTICS AND SPACE ADMINISTRATION  
Washington, D.C. 20546